NATIONAL ADVISORY COMMITTEE FOR AERONAUTICS

TECHNICAL MEMORANDUM 1427

TURBULENCE IN THE WAKE OF A THIN AIRFOIL AT LOW SPEEDS

By George S. Campbell

California Institute of Technology

Washington

January 1957

NATIONAL ADVISORY COMMITTEE FOR AERONAUTICS

TECHNICAL MEMORANDUM 1427

TURBULENCE IN THE WAKE OF A THIN AIRFOIL AT LOW SPEEDS

By George S. Campbell

SUMMARY

Experiments have been made to determine the nature of turbulence in the wake of a two-dimensional airfoil at low speeds. The experiments were motivated by the need for data which can be used for analysis of the tail-buffeting problem in aircraft design. Turbulent intensity and power spectra of the velocity fluctuations were measured at a Reynolds number of 1.6×10^5 for several angles of attack. Total-head measurements were also obtained in an attempt to relate steady and fluctuating wake properties.

Mean-square downwash was found to have nearly the same dependence on vertical position in the wake as that shown by total-head loss. For this particular wing, turbulent intensity, integrated across the wake, increased roughly as the 3/2 power of the drag coefficient.

Power-spectrum measurements indicated a decrease in frequency as wing angle of attack was increased. The average frequency in the wake was proportional to the ratio of mean wake velocity to wake width.

INTRODUCTION

The study of velocity fluctuations in the wake of an airfoil is of interest in connection with the buffeting problem. In one form of buffeting, referred to as tail buffeting, the horizontal tail of the aircraft is immersed in the wake of the wing for certain angles of attack. If the wake contains sufficient turbulent energy, as it may due to separated flow over the wing, the aircraft may experience undesirable load fluctuations. It might be mentioned that buffeting is not always undesirable, as it is often useful as an advance warning against dangerous stability deficiencies.

A recent book on aeroelasticity (ref. 1) has summarized the results of some investigations of tail buffeting. From this summary, it appears that there has been considerable work done on buffeting

for high angles of attack, but that there is little information available on the possibility of buffeting at lower angles. The use of increasingly thinner wing sections introduces the likelihood of leading-edge separation at low angles of attack (ref. 2). Although this type of separation usually disappears at transonic Mach numbers, it is generally replaced by separation behind the main compression shock. In either case, the occurrence of such separated flows at low angles of attack would be expected to cause buffeting difficulties.

A useful approach for the study of most of the various types of tail buffeting has been provided in reference 3. In this paper, buffeting was considered to be the response of a linear system to a random forcing function. In order to predict the response of an elastic structure to turbulent velocity fluctuations, one must know the power spectrum of the turbulence, the aerodynamic impedance of the lifting surface, and the frequency response of the structure. Nonstationary wing theory may be used to estimate the aerodynamic impedance functions of various lifting surfaces[1]. The determination of the frequency-response characteristics of aircraft structures has received sufficient attention over a period of years so that this portion of the buffeting problem may be considered solved. The remaining quantity necessary for the analysis of tail buffeting is the power spectrum of turbulence in the wake of the forward lifting surface. Up to the present time, it has been necessary to assume that the turbulence is isotropic or that it possesses a discrete frequency corresponding to a Kármán vortex street. However, it is evident that measurements of the power spectra of turbulence behind wings are necessary before the general statistical approach to buffeting can be fully utilized.

The primary purpose of the present investigation has been the measurement at low speeds of the power spectrum of turbulence behind a thin, two-dimensional airfoil. The tests were made by means of the usual hot-wire techniques for measuring velocity fluctuations in turbulent flow (ref. 5). Angle of attack was varied from 0 to 22 degrees, and the Reynolds number for most of the tests was about 1.6×10^5. It might be expected that the results could be applied at higher Reynolds numbers provided the wing exhibits the type of leading-edge separation shown by the airfoil in the present tests. Total-head surveys and surface-tuft studies were made in order to determine the static characteristics of the wing and its wake. Wherever possible, an attempt has been made to relate the power spectrum of turbulence to the mean properties of the flow.

---

[1]A recent experimental investigation (ref. 4) confirms, in general, the applicability of classical nonstationary wing theory when the velocity fluctuations are of a random nature.

This research was conducted at the California Institute of Technology under the guidance of H. W. Liepmann while the author was a holder of a Howard Hughes Fellowship.

APPARATUS AND TESTS

Wind Tunnel

The experiments of this investigation were made in the GALCIT 20- by 20-inch low turbulence wind tunnel; a diagram of the tunnel is presented in reference 6. The turbulence level of the tunnel is about 0.03 percent.

Most of the present tests were conducted at velocities of about 50 feet per second. Free-stream velocity was, in general, measured using a pitot-static tube and a micromanometer. At lower speeds, however, it was found convenient to measure velocity by observing on an oscilloscope the frequency of vortices shed from a reference cylinder. A description of this procedure is given in reference 7.

The traverse mechanism for positioning hot-wire and total-head probes is the same as the one described in reference 7.

Airfoil

A two-dimensional airfoil of 6-inch chord spanned the test section. The airfoil section was a 1/8-inch thick flat plate with a blunt trailing edge and a rounded nose. The leading-edge radius was approximately half the airfoil thickness. The wing was made of steel and was tested in a smooth condition.

All measurements were made behind the center section of the wing span. Reynolds number for most of the tests was about 1.6×10^5.

Total-Head Surveys

A total-head survey of the wake was made one chord length behind the wing trailing edge using a total-head tube of 0.108-inch outer diameter. Profile-drag coefficient was obtained by integrating the total-head profile

$$C_D = \int \frac{\Delta H}{q} d\left(\frac{z}{c}\right) \tag{1}$$

This formula is expected to give quite satisfactory accuracy with the survey plane one chord from the trailing edge (ref. 8).

Hot-Wire Apparatus

The usual methods of hot-wire anemometry (ref. 5) were used to measure fluctuating velocities in the airfoil wake. Hot wires of 0.1 mil platinum or platinum-rhodium were used for all measurements. For measurements of the longitudinal velocity fluctuation, u^2, a 1/8-inch long wire was soldered to the tips of the probe. Transverse velocity fluctuations were obtained with a probe having two wires of 0.2 inch length inclined at angles of $\pm$ 30 degrees from the stream direction.

A considerable saving in testing time was accomplished by omitting hot-wire calibrations. Reliable relative measurements of the turbulent velocity fluctuations could be obtained in this manner provided the hot-wire apparatus was linear. It is estimated on the basis of data from reference 9 that the downwash probes of the present investigation should be linear for fluctuations up to about $\pm 25^{\circ}$. The overall linearity of the hot-wire apparatus was checked by observation of oscilloscope traces of the hot-wire output. The presence of nonlinearities (such as those which could be introduced by excessively high amplifier gains) generally resulted in flat tops to an otherwise random oscillograph trace.

The frequency response of the amplifier used for the hot-wire measurements was flat for frequencies of 1/2 to 25,000 cycles per second. The post-amplifier was provided with resistance-capacitance compensation which was adjusted by the usual square-wave method. In order to minimize noise a 10 kilocycle cut-off filter was used in the present measurements.

Electronic Measurements

Intensity of the turbulent velocity fluctuations was determined by means of an average-reading vacuum-tube voltmeter. Although the voltmeter was calibrated to give RMS values for sinusoidal voltage variations, the instrument did not provide true RMS intensities for random inputs. On the basis of turbulence measurements with a statistical analyzer (ref. 7), the difference between true and indicated RMS is expected to be less than 10 percent.

Power-spectral density was measured with a Hewlett-Packard model 300A wave analyzer. A constant half-band width of 30 cycles per second, based on an attenuation of 40 decibels, was used for all measurements.

The filtering characteristics of the wave analyzer are shown in figure 1 for the 30 cycle band width. The frequency range of the analyzer was about 30 - 16,000 cycles per second. The output was read directly from the instrument's voltmeter, and so the values obtained were subject to the same errors for random inputs as were the intensity measurements described in the previous paragraph.

ACCURACY

Fan Frequency

Of the factors affecting the accuracy of measurements of power-spectral density, the rotational speed of the wind-tunnel fan is one of the most important. The motor and fan were quite well isolated from the test section so that vibrations were not transmitted to the hot-wire mount. However, periodic pressure fluctuations were found to be transmitted upstream, and so a test was made to determine the effect of tunnel fan rotation on power-spectrum measurements. Downwash velocities are of primary interest, and so downwash spectra are compared in figure 2 for two fan speeds. The same free-stream velocity was maintained by introducing a screen just ahead of the fan for one of the tests. Without the screen, the peak in the downwash spectrum occurs at nearly the same frequency as the fan's second harmonic. However, the downwash spectrum has practically the same shape when the fan and wing peaks do not coincide, i.e., when the screen is added. Therefore, it may be concluded that the fan is not the cause of the peak in the downwash spectrum, even though it does somewhat modify the spectrum.

Noise

The noise introduced by the measuring apparatus was generally small and was subtracted from the total output. Near the center of the wake, the ratio of signal to noise was greater than 100 to 1 for RMS turbulent intensity. Measurements at 60 cycles per second were usually high by about 3 percent due to pickup of line frequency. The greatest uncertainty in the spectrum measurements occurred at the lowest frequency, 30 cycles per second, due to the characteristics of the wave analyzer.

Wall Interference

On the basis of an analysis by Glauert (ref. 10), the Strouhal number of the vortex street obtained at an angle of attack of 21.7 degrees in the present investigation should be about 6 percent higher

than the value obtained in a stream of unlimited extent. This is also the magnitude of the correction necessary to bring the present results into agreement with those of Fage and Johansen (ref. 11), obtained for the same size model in a much larger tunnel. The corrections to Strouhal number at lower angles of attack are proportionately smaller. It appears that wall corrections for power spectra and turbulent intensities are not presently available. In order to have consistency between Strouhal numbers and power spectra, all data are therefore presented without applying any corrections for wind-tunnel wall interference.

Hot-Wire Length Corrections

The general effect of the finite length of a hot wire is to reduce the voltage across the wire as a result of imperfect correlation of the velocity fluctuations at different points of the wire. For isotropic turbulence, estimates of the corrections to intensity may be quite simply obtained (references 12 and 13, for example). In experimental measurements of the spectrum of turbulence behind grids (ref. 6), corrections to the power-spectral density were found negligible for reasonable hot-wire lengths. Unfortunately, the estimation of length corrections for the present investigation is greatly complicated by the use of a two-wire probe in a field which bears scant resemblance to isotropic turbulence. In view of this uncertainty, length corrections have not been applied to the data.

RESULTS

Wake Energy Distribution

Two measures of wake energy were obtained in the present investigation: total-head loss and the mean-square of the downwash fluctuations. As total-head measurements are considerably simpler than hot-wire studies, it is desirable to determine whether properties of the turbulent flow can be related to the simpler mean flow.

Presented in figures 3-7 are the wake profiles obtained from total-head and hot-wire surveys at a distance of one chord length from the wing trailing edge. The profiles have been normalized to unit area; the position of the trailing edge relative to the wake center is indicated on the curves. It is seen from these results that the shape of the turbulent velocity profiles closely resembles that of the total-head profiles. The main differences are the more gradual decay of the turbulent velocities at the outer edges of the wake and the somewhat sharper peaks for the total-head loss.

Wake widths from figures 3-7 have been plotted as a function of angle of attack in figure 8. In defining wake width, the edge of the wake is arbitrarily taken as the point at which total-head loss or $\overline{w^2}$ is one-tenth of the maximum value. It is seen from figure 8 that the wake widths obtained from the total-head survey and the $\overline{w^2}$ measurements are in close agreement for the angle-of-attack range investigated. It should be mentioned that wake widths based on profiles of the RMS turbulent velocity, $\sqrt{\overline{w^2}}$, would necessarily be larger than the present wake widths, which are based on the mean-square velocity.

A comparison of the total-head profiles for angles of attack from 0 to 14 degrees is presented in figure 9. A similar comparison for the $\overline{w^2}$ measurements is given in figure 10. For both total head and $\overline{w^2}$ the profile shapes exhibit approximate similarity for the angle-of-attack range investigated.

Variation of the wing drag coefficient with angle of attack is shown in figure 11. This result was obtained by integration of the total-head profiles measured one chord length behind the wing trailing edge. The abrupt rise in drag in the vicinity of 3 degrees angle of attack apparently results from separation of the boundary layer at the leading edge of the wing. It was observed during a limited tuft study that flow was extremely irregular over the entire upper surface of the wing at 6 degrees incidence. Flow over the wing was smooth at 2 degrees except for a small region of moderately irregular flow at the leading edge.

Variation of the relative intensity of the downwash fluctuations with angle of attack is presented in figure 12. These values were obtained by integrating the $\overline{w^2}$ profiles measured one chord length behind the wing trailing edge. The intensity of the downwash fluctuations increased sharply at the higher angles of attack, probably due to the occurrence of leading-edge separation, as previously discussed.

Turbulent downwash intensity is shown as a function of drag coefficient in figure 13. Integrated $\overline{w^2}$ intensity increased approximately with the 3/2 power of the drag coefficient in these tests. When the local intensity at a given point in the wake, such as the wake center, is plotted against drag, the variation is nearly linear. A large part of the increase in integrated intensity is due to the broadening of the wake at the higher angles of attack.

Power Spectra of the Downwash Fluctuations

Effect of angle of attack and wake position. - The results of measurements of the power spectra of the downwash fluctuations one chord length behind the wing trailing edge are presented in figures 14 to 20 for angles of attack from 0 to 14 degrees. In general, the power spectrum was measured directly behind the wing trailing edge and also at the outer edge of the wing wake at each angle of attack. The relative height of the turbulent trace for the two positions in the wake may be seen from the wake profile of RMS downwash at the top of each figure. The vertical tics on the wake profiles show the position at which power spectra were measured.

A constant half-band width of 30 cycles per second, based on 40 decibels attenuation, was used for all spectrum measurements. The filtering characteristics of the wave analyzer are shown in figure 1.

From figures 14 to 20 it is seen that wing angle of attack has an important effect on the power spectrum of the downwash velocity. The spectrum at zero incidence (fig. 14) is dominated by the discrete frequency corresponding to a vortex street shed from the blunt trailing edge of the wing. At 3-1/2 degrees angle of attack, the trailing edge vortex street is still apparent, but the bulk of the turbulent energy is spread over a broad band of frequencies.

With further increase in angle of attack, the downwash spectrum near the wake center shows a progressive decrease in the predominant frequencies. The bulk of the turbulent energy is concentrated near the wake center, and so a general conclusion from this data is that wake frequency decreases as wing incidence is increased.

By 14 degrees angle of attack (fig. 20), a vortex street is formed behind the stalled wing, and the measured spectrum corresponds essentially to a delta function which is spread out by the finite band width of the wave analyzer (fig. 1). At first thought, it seems unusual that the frequency measured near the center of the vortex street is not double the frequency at the wake edges because of the influence of both rows of the vortex street. Therefore, a calculation of the velocities induced by a vortex street was made using the equations of reference 14. The results are presented in figure 21, along with the geometry of the assumed vortex street. The upper graph in figure 21 gives the variation of the longitudinal induced velocity, u, with distance along the vortex street, and the lower graph presents the variation of induced downwash, -w. The induced velocities were calculated along the center of the vortex street ($z = 0$) and also along a line located above the vortex street ($z = b$). As expected, the predominant frequency of the u velocity in the center of the wake is double the frequency outside the vortex street. However, the downwash velocity in the wake center does not show frequency doubling; this result is in agreement with the measurements of

the downwash power spectrum presented in figure 20.

Below the stalling incidence, the downwash spectrum is much broader near the center of the wake than at the outer edge of the wake. Moreover, the predominant frequencies at the edge of the wake are practically independent of wing incidence for angles of attack from 6 to 14 degrees. Because there is very little turbulent energy in the outer edges of the wake, subsequent analysis of the data will be, for the most part, based on the spectrum measurements directly behind the wing trailing edge ($z = 0$).

Relation between frequency and wake width. The data presented in figures 14 to 20 show that the predominant frequencies in the wing wake generally decrease as the wake width increases. In order to illustrate this result more explicitly, it is convenient to define an average frequency for the turbulent power spectrum. The average wake frequency, n_{av}, is defined as the frequency which divides a power spectrum into two equal areas. In figure 22 the reciprocal of the average wake frequency is plotted against an effective wake width, defined as the wake width divided by average wake velocity. The experiments show that the average wake frequency is inversely proportional to the effective wake width. In other words, a non-dimensional frequency or Strouhal number based on wake width and wake velocity is nearly constant. This result is in agreement with a recent correlation based on free-streamline theory for a series of bluff bodies (ref. 15).

A line labeled "instability theory" in figure 22 was calculated using the instability theory of wakes presented in reference 16. The possibility of applying stability theory to a turbulent velocity profile has never been fully discussed.[2] Instability of laminar shear flows generally implies the eventual formation of a turbulent flow. When the flow is already turbulent, the meaning of an instability calculation is far from clear. However, even in laminar flow only the very beginning of instability can be handled by a linear theory; it is not impossible that the application of similar considerations to turbulent flow could provide interesting results. For example, it is known that Kármán vortex streets and three-dimensional Taylor vortices may exist even in turbulent flow. Therefore, it is interesting to compute the frequencies predicted for neutral stability and to compare these frequencies with the measured results, as in figure 22. Instability theory predicts the same inverse relationship between frequency and effective wake width shown by the experimental measurements. Although the actual magnitude of the predicted frequency is

[2] A few remarks concerning the existence of a large-scale structure in turbulent shear flows have been made in reference 13.

in close agreement with the measured results, this is very likely coincidental. First of all, the theory assumes neutrally stable disturbances whereas amplified disturbances would probably be more important in any real flow. Also, different average frequencies could be obtained from the measured spectra depending on the method chosen to define an average. Details of the stability calculation are presented in Appendix B.

Relation between frequency and projected wing chord. - It has been observed in several investigations that the Strouhal number based on the projected chord of a wing is nearly constant for angles of attack above the stall (ref. 1). In order to determine whether such a constant Strouhal number is obtained for smaller angles of attack, the average wake frequencies, n_{av}, obtained from measured power spectra are shown in figure 23 as a function of projected airfoil breadth. This projected breadth is defined as the total airfoil projection, which includes the finite thickness of the wing. The line labeled "empirical" corresponds to a constant projected Strouhal number obtained by extrapolating the frequency measured for the stalled wing ($\alpha = 14^\circ$).

The empirical extrapolation gives a reasonable prediction of the average wake frequency except for an angle of attack of 3-1/2 degrees. At this angle of attack the airfoil does not have the leading-edge separation that occurred at higher angles, and so it is not surprising that wake frequency is not related to projected chord. When frequency is related to wake width instead of projected chord, the unseparated flow condition does not present this difficulty. Therefore, it appears that wake width is more suitable than projected chord for correlating frequency measurements.

Power Spectra of the Longitudinal and Spanwise Velocities

Although downwash fluctuations are generally more effective as a cause of buffeting loads, the power spectra of the longitudinal and spanwise velocities are necessary for more complete understanding of turbulent wakes. Longitudinal velocity spectra were measured for an angle of attack of 6 degrees at several vertical positions in the wake, and the results are shown in figures 24 and 25. The corresponding downwash spectra are presented in figures 26 and 27.

Looking at the data as a whole, the u^2 and w^2 power spectra generally have pronounced maxima at values of $\frac{nc}{U_\infty} = 0.65$ or 1.30. The u^2 and w^2 spectra are similar to each other over the outer portion of the wake, but the spectra are markedly different near the wake center.

In order to determine whether the wing wake resembles a vortex street at this angle of attack, the velocities induced by a vortex street (fig. 21) were expressed in terms of their Fourier coefficients. The resulting harmonic analysis of an idealized vortex street is presented in figure 28 for several vertical locations above the center of the vortex street. The first and second Fourier coefficients for the u velocity are on the left of the figure, and the corresponding downwash coefficients are on the right. Comparing the calculated results with the measurements given in figures 24 to 27, it is seen that the measured data do not show consistent agreement with the calculations. Therefore, it seems likely that the structure of the wing wake at low angles of attack is more complicated than that of a simple vortex street.

In figure 29 the u^2 spectrum directly behind the wing trailing edge is compared with the spectrum of the spanwise velocity component. These spectra may be compared with the spectra for isotropic turbulence. The longitudinal or u^2 spectrum of isotropic turbulence has been obtained experimentally in the investigations of references 6 and 17. From such results the transverse spectra may be calculated using the continuity relation for isotropic turbulence (ref. 18). Measurements of the longitudinal spectrum may be approximated by the relation

$$F_1(n) = \frac{4L}{U_\infty} \frac{1}{(1 + \xi^2)} \tag{2}$$

and the corresponding transverse spectrum is

$$F_2(n) = \frac{2L}{U_\infty} \frac{(1 + 3\xi^2)}{(1 + \xi^2)^2} \tag{3}$$

The variable ξ is a non-dimensional frequency given by

$$\xi = \frac{\omega L}{U_\infty} \tag{4}$$

and L is the turbulent macroscale of the longitudinal velocity

$$L = \frac{U_\infty F_1(0)}{4} \tag{5}$$

The isotropic power spectra shown in figure 30 were calculated for the same value of L as that measured in the wing wake, figure 29. Comparison of figures 29 and 30 indicates that the u^2 and v^2 spectra near the center of the wing wake are similar, respectively, to the longitudinal and transverse spectra of isotropic turbulence. This similarity was not shown at other vertical positions in the wake, although part of the total turbulent energy may still be attributable to an isotropic-like turbulence.

Effect of Free-Stream Velocity

The results presented so far were obtained at a free-stream velocity of about 50 feet per second. In order to determine whether the results may be used for other free-stream velocities, representative tests were made at a lower velocity. These additional tests do not provide significant information on the effect of Reynolds number variation, but should facilitate interpretation of the results. For example, it is generally assumed that aerodynamic frequencies are proportional to velocity, and so this assumption should be checked.

Wake-energy distribution. - The fluctuating-downwash profile is shown in figure 31 for velocities of 30 and 49 feet per second. Although the profile is somewhat steeper for the lower velocity, the wake width is practically unaffected by the velocity change. The overall effect of the velocity change on the profile is negligible.

Discrete frequencies. - The effect of velocity on the periodic wake behind the blunt trailing edge of the flat-plate airfoil is shown in figure 32 for zero angle of attack. At the higher velocities, frequency is proportional to velocity. The Strouhal number, $\frac{nt}{U_\infty}$, of the fluctuations, based on trailing-edge thickness, is 0.24, which is in good agreement with the Strouhal number of 0.23 obtained in reference 19 from schlieren observations of the vortex street behind a blunt trailing-edge airfoil. For velocities below about 20 feet per second (fig. 32), the frequencies in the wing wake become nonlinear with velocity. This corresponds to a decrease in Strouhal number for Reynolds numbers below 10^3, with Reynolds number based on trailing-edge thickness. The Strouhal number of a cylinder also shows a decrease for Reynolds numbers below 10^3. (See fig. 149, ref. 20.)

Velocity fluctuations in the wake were also periodic above the stalling angle of the wing. The effect of free-stream velocity on wake frequency is shown in figure 33 for two angles of attack. Over the

Reynolds number range of these tests, frequency is proportional to velocity. The Strouhal number based on projected chord is 0.19 for $\alpha = 14.5^\circ$ and 0.18 for $\alpha = 21.7^\circ$. In the discussion of the accuracy of measurements, it was noted that these frequencies are probably slightly high due to wall interference. Nevertheless, the values are well within the range of Strouhal numbers obtained in various investigations of vortex streets behind stalled plates and airfoils (ref. 1).

Power spectra. - The power spectrum of downwash fluctuations behind the wing at a moderate angle of attack is shown in figure 34 for two values of the free-stream velocity. Roughly speaking, the normalized power-spectral density is uniquely dependent on the usual frequency parameter, $\frac{nc}{U_\infty}$, for the two velocities. Some of the disagreement between the two spectra very likely results from the replacement of hot-wires during the interval between the two tests. In any case, the overall agreement of the spectra appears quite satisfactory.

DISCUSSION

Prediction of RMS Lift in Tail Buffeting

Formulas for the prediction of the RMS lift fluctuations on a tail surface located in a turbulent wake have been given in reference 21. However, in order to obtain explicit results, it was necessary to assume that the turbulence striking the tail surface was isotropic. The effect of this assumption may be evaluated by using an actual power spectrum measured in these tests to calculate RMS lift on a hypothetical tail surface.

A convenient relation for calculating mean-square lift was derived in reference 21, and, except for a slight difference in notation, the relation is:

$$\overline{C_L^2} = 4\pi^2\overline{\alpha^2}\int_0^\infty F(n)\left|\phi(k)\right|^2 dn \qquad (6)$$

The assumptions on which this equation is based are: (1) the tail aerodynamics may be described by a two-dimensional admittance function, $\phi(k)$; (2) the scale of turbulence is large compared with the tail span.

It is evident from equation 6 that certain parameters, such as

velocity and wing chord, must be assumed in order to calculate the mean-square lift coefficient. However, the minimum number of assumptions are made if equation 6 is modified so as to incorporate a useful similarity property of the power spectrum; namely, that

$$\frac{U_\infty F(n)}{c} = fn\left(\frac{nc}{U_\infty}\right) \tag{7}$$

as seen from figure 34. Then equation 6 becomes

$$\frac{\overline{C_L^2}}{4\pi^2\overline{\alpha^2}} = \int_0^\infty fn\left(\frac{nc}{U_\infty}\right) \left| \phi\left(\frac{c_t}{c}\,\frac{nc}{U_\infty}\right)\right|^2 d\left(\frac{nc}{U_\infty}\right) \tag{8}$$

The object of the lift calculation may now be described more explicitly. Using the same tail surface and aerodynamic admittance function, $\overline{C_L^2}/\overline{\alpha^2}$ is to be calculated for a power spectrum measured behind the wing (fig. 17, z = 0) and compared with a similar result calculated for the transverse isotropic spectrum (fig. 30). The aerodynamic admittance of a tail having $c_t/c = 0.2$ was calculated using equation 13 of reference 3, and the result is shown in figure 35. For this tail surface, the comparison of RMS lift for an actual wing downwash spectrum with the RMS lift for isotropic turbulence is as follows:

SPECTRUM	$\frac{1}{2\pi}\sqrt{\frac{\overline{C_L^2}}{\overline{\alpha^2}}}$
Wing	0.37
Isotropic	0.41

From this comparison, it is evident that the exact shape of the turbulent power spectrum has a relatively small effect on the mean lift fluctuations experienced by a tail surface. A simple closed-form expression is available for calculating $\overline{C_L^2}/\overline{\alpha^2}$ in isotropic turbulence (equation 28 of reference 21), and the above comparison shows that this equation should be quite useful for predicting the RMS lift on a tail in the wake of a wing. However, in order to apply the formula, it is necessary to estimate the macroscale of the turbulence striking the tail surface. For the comparison just presented, the turbulent scale was obtained from a measured u^2 spectrum using equation 5. Such results are not usually available to designers, and so it is necessary to have a simpler means of estimating the scale of turbulence in a wing wake. A possible method for obtaining such an estimate will now be discussed.

The turbulent scale, L, may be used to define a characteristic frequency by simple dimensional analysis:

$$n = \frac{U_\infty}{2\pi L} \tag{9}$$

It might be expected that this frequency would correspond to the predominant frequency in the turbulence, and this assumption may be checked using the data of the present tests. The characteristic frequency calculated from the u^2 spectrum of figure 29 and equation 9 was found to be $nc/U_\infty = 1.24$. This frequency corresponds almost exactly to the predominant frequency in the w^2 power spectrum, figure 17. Therefore, equation 9 provides a simple means of estimating turbulent scale because wake frequencies can be obtained more easily than a power spectrum. For example, a tuft probe could be placed in the wing wake and the mean frequency could then be obtained from motion pictures of the tuft movement.

Buffeting Measurements with Detector Airfoils

From the results of some earlier investigations of tail buffeting (ref. 22, 23), it was concluded that lift fluctuations may be obtained well outside the limits of the total-head wake. This result appears to be at variance with the present investigation and that of reference 24. Therefore, it seems worthwhile to discuss the reasons for the different conclusions.

The fact that relatively strong lift fluctuations have been

detected beyond the region of the total-head wake is not surprising for several reasons. First, the intensity of the fluctuations observed in references 22 and 23 was taken, roughly speaking, as the maximum amplitude of the detector airfoils. Therefore, the data obtained in this manner represent an upper limit of the lift fluctuations and do not necessarily represent a statistical average of the fluctuations. In the present investigation, it was generally observed that near the edge of the total-head wake, occasional bursts of turbulence were found to be notably larger than the general level of the turbulent velocity fluctuations. When such bursts occur in the outer edges of the wake, a wake width based on maximum values would be larger than the width obtained from statistically averaged data.

Even in the absence of such bursts, the profiles in references 22 and 23 would be broader than those of the present report as only the latter are expressed in terms of mean-square fluctuations. The profiles of references 22 and 23 correspond more nearly to RMS fluctuations, and RMS values must necessarily fall off more rapidly than mean squares.

Finally it is noted that the predominant velocity fluctuations near the center of the wake occur at higher frequencies than those observed at the wake edges (figs. 26 and 27). Because low frequency velocity fluctuations are more effectively converted to lift fluctuations (ref. 3), the lower frequencies found in the outer portions of a wake are less attenuated than the high frequency energy in the wake center. This effect supplies another contributing cause for the breadth of the fluctuating lift profiles presented in references 22 and 23.

In order to illustrate the effects just discussed, representative data obtained in the present investigation have been shown in several different forms in figures 36 to 38. Using the measured power spectra for the downwash fluctuations, figure 36, the frequency distribution of RMS lift has been estimated for an airfoil located at various heights in the wing wake. The simulated horizontal tail had a chord equal to 20 percent of the wing chord. The form of the approximate admittance function used to calculate lift spectra is shown in figure 35. On the basis of results from reference 4, it is expected that such an admittance function is representative of the admittance of the sensitive airfoils used by Ferri (ref. 23). The resulting frequency distribution of RMS lift estimated in this manner is presented in figure 38. A comparison of the relative intensities obtained from the RMS lift spectra (fig. 38) and the conventional angularity spectra (fig. 36) is as follows:

z/c	$\overline{w^2}$	$\sqrt{\overline{C_L^2}}$
0	1.000	1.000
.22	.305	.551
.48	.004	.051

From this result, it is seen that tests using sensitive airfoils would be expected to indicate greater wake widths than those obtained from hot-wire surveys. The occurrence of bursts, as previously discussed, could cause even greater differences between lift and angularity data.

CONCLUSIONS

1. The mean square of the downwash fluctuations was found to have approximately the same variation with vertical position in the wing wake as that shown by measurements of total-head loss.

2. The intensity of downwash fluctuations increased rapidly when the flow separated from the wing surface. For the present tests, integrated downwash intensity increased with approximately the 3/2 power of wing drag coefficient.

3. Power spectra for the downwash velocity were generally broader at the low angles of attack than at high angles. The average frequency in the wake was proportional to the ratio of wake velocity to wake width. Wake width appears to be a more suitable parameter for correlating spectrum measurements than the projected airfoil chord.

4. The outer edges of the wing wake contained relatively little high-frequency energy, whereas the turbulent energy near the wake center was distributed over a fairly wide range of frequencies.

5. The wake structure at low angles of attack appears to be much more complicated than for the stalled airfoil, for which a vortex street forms behind the wing.

6. Power spectra measured at different velocities were found to be similar when frequency and power spectral density were nondimensionalized by the ratio of airfoil chord to free-stream velocity, c/U_∞.

7. On the basis of calculated results, the exact shape of the turbulent power spectrum was found to have a relatively small effect on the RMS lift of a tail surface located in the wake of the wing. Formulas for predicting lift assuming isotropic turbulence should give satisfactory results if the turbulent scale is correctly estimated.

APPENDIX A

Symbols

The following symbols are defined as they are used in the main body of this paper. Certain letters have been used with different meaning within Appendix B in order to retain the notation of reference 16.

a	distance between vortices in the same row
b	breadth of vortex street
C_D	drag coefficient, $\frac{\text{drag/span}}{qc}$
C_L	lift coefficient, $\frac{\text{lift/span}}{qc}$
c	airfoil chord
$F(n)$	power spectral density of a random variable; $F(n) = 4\int_0^\infty R(\tau)\cos 2\pi n\tau \, d\tau$
$F_1(n)$	power spectral density for longitudinal velocity in isotropic turbulence
$F_2(n)$	power spectral density for transverse velocity in isotropic turbulence
k	reduced frequency, $\omega c/2U_\infty$
L	turbulent macroscale, equation 5
n	frequency, cycles/second

n_1 the first harmonic frequency of a vortex street

n_{av} average wake frequency, defined as the frequency which divides a power spectrum into two equal areas

q dynamic pressure, $\frac{1}{2}\rho U_\infty^2$

$R(\tau)$ time-correlation function of a random variable;

$$R(\tau) = \overline{u(t)\, u(t+\tau)} / \overline{u^2}$$

$$R(\tau) = \int_0^\infty F(n) \cos 2\pi n\tau \, dn$$

TE trailing edge

t wing thickness

U_∞ free-stream velocity

u longitudinal perturbation velocity

v spanwise perturbation velocity

w vertical perturbation velocity

W wake width

x distance along stream direction from wing trailing edge

z vertical distance above centerline of wing trailing edge

α angle of attack

Γ vortex strength

ΔH difference between free-stream and local total head

ζ height above wake center

ξ non-dimensional frequency, $\omega L/U_\infty$

ρ free stream density

τ time

$\phi(k)$ ratio of lift at frequency k to lift at zero frequency

ω circular frequency, $2\pi n$

APPENDIX B

Application of Stability Theory to the Prediction of Wake Frequencies

In this appendix assumptions underlying the stability theory of wakes (ref. 16) are briefly outlined. Also, certain additional formulas are developed in order to facilitate comparison between theory and experiment.

Hollingdale (ref. 16) considers a mean wake flow whose velocity relative to the stream at infinity is

$$\left.\begin{aligned} u &= U(z) \\ v &= 0 \\ w &= 0 \end{aligned}\right\} \tag{B1}$$

With the assumption of small two-dimensional disturbances a linear, homogeneous equation for the disturbance velocities is obtained from the incompressible Navier-Stokes equations. The stream function ψ may be assumed periodic, so that

$$\psi = \phi(z)e^{i\alpha(x-ct)} \tag{B2}$$

The wave length of the disturbance is $2\pi/\alpha$, and c is the wave velocity. The basic equation for determining the stability of small disturbances in a wake or other region of shear flow is then

$$(U - c)(\phi'' - \alpha^2\phi) - U''\phi = \frac{\nu}{i\alpha}(\phi^{IV} - 2\alpha^2\phi'' + \alpha^4\phi) \tag{B3}$$

From the complete stability equation B3 Hollingdale has determined that the wave velocity c for an undamped disturbance is equal to the value of U at the point of inflection of the velocity profile U(z). This result is valid for symmetrical or monotonic profiles in which U approaches a constant for large z.

For sufficiently large Reynolds numbers the viscous terms of equation B3 may be omitted:

$$(U - c)(\phi'' - \alpha^2\phi) - U''\phi = 0 \tag{B4}$$

The velocity profile may be assumed to be of the form

$$\begin{aligned} U &= A(1 + \cos kz) && 0 \leq |z| \leq \pi/k \\ U &= 0 && |z| > \pi/k \end{aligned} \tag{B5}$$

where π/k is the wake semiwidth, subsequently denoted as $W/2$. The constant A must equal the wave velocity in order that $U = c$ at the point of inflection $U'' = 0$. For the particular form of profile chosen the stream function must therefore satisfy the relations

$$\begin{aligned} \phi'' + (k^2 - \alpha^2)\phi &= 0 && 0 \leq |z| \leq \pi/k \\ \phi'' - \alpha^2\phi &= 0 && |z| > \pi/k \end{aligned} \tag{B6}$$

The boundary conditions to be satisfied by ϕ are that it is an even function in the region $\left(-\frac{\pi}{k}, \frac{\pi}{k}\right)$ and that it approaches zero for large z. Solutions satisfying these conditions and the differential equations B6 are

$$\begin{aligned} \phi &= P \cos \sqrt{k^2 - \alpha^2}\, z && 0 \leq |z| \leq \pi/k \\ \phi &= Qe^{-\alpha|z|} && |z| > \pi/k \end{aligned} \tag{B7}$$

These equations provide the characteristic equation for determining the wave-length parameter α if ϕ and ϕ' are required to be continuous at $|z| = \pi/k$:

$$\tan \frac{\pi\sqrt{k^2 - \alpha^2}}{k} = \frac{\alpha}{\sqrt{k^2 - \alpha^2}} \tag{B8}$$

The parameter

$$\sigma = \frac{a}{k} = \frac{W}{2\pi/a} \tag{B9}$$

is simply the ratio of the wake width to the wave length of the disturbance. The important result from equation B8 is that this ratio is a constant and, in fact, has the numerical value

$$\sigma = 0.926 \tag{B10}$$

Disturbance waves of the type predicted by Hollingdale reach a point which is fixed relative to the body producing the wake with the frequency

$$n = \frac{a}{2\pi} (U_\infty - A) \tag{B11}$$

where U_∞ is the free-stream velocity and A is the wave velocity. Introducing Hollingdale's result for the proportionality between wave length and wake width, equation B9, provides the expression for the frequency of small periodic disturbances:

$$n = \frac{(U_\infty - A)\,\sigma}{W} \tag{B12}$$

Although the value of the wave velocity A may be determined as the velocity at the point of inflection of the velocity profile, it is difficult in practice to determine the inflection point of an experimental velocity profile. Hence, it is desirable to have a more practical method of estimating wave velocity. The drag may be obtained by integration of the total-head loss if the survey plane is a sufficient distance from the wing trailing edge:

$$C_D = \int \frac{\Delta H}{q} \, d\left(\frac{z}{c}\right) \tag{B13}$$

The relation between total-head loss and the velocity deficit U in the wake may be obtained from Bernoulli's equation by assuming the static pressure in the wake is equal to the free-stream pressure.

$$\frac{\Delta H}{q} = \frac{U}{U_\infty}\left(2 - \frac{U}{U_\infty}\right) \tag{B14}$$

When equation B5 for the velocity variation, is substituted into equations B13 and B14, a relation for the wave velocity in terms of drag and wake width is obtained:

$$\frac{3}{2}\frac{A}{U_\infty} = 1 - \sqrt{1 - \frac{3}{2}\frac{C_D c}{W}} \tag{B15}$$

REFERENCES

1. Fung, Y. C.: An Introduction to the Theory of Aeroelasticity. John Wiley and Sons, Inc., 1955.

2. Lindsey, W. F., Daley, B. N., and Humphreys, M. D.: The Flow and Force Characteristics of Supersonic Airfoils at High Subsonic Speeds. NACA TN 1211, 1947.

3. Liepmann, H. W.: On the Application of Statistical Concepts to the Buffeting Problem. Jour. Aero. Sci., vol. 19, no. 12, pp. 793-801, Dec. 1952.

4. Lamson, P.: Measurements of Lift Fluctuations Due to Turbulence. CIT, Ph.D. Thesis (to be published by the NACA), 1956.

5. Willis, J. B.: Review of Hot Wire Anemometry. Australian A. C. A. 19, 1945.

6. Liepmann, H. W., Laufer, J., and Liepmann, K.: On the Spectrum of Isotropic Turbulence. NACA TN 2473, 1951.

7. Roshko, A.: On the Development of Turbulent Wakes from Vortex Streets. NACA TN 2913, 1953.

8. Fage, A., and Jones, L. J.: On the Drag of an Aerofoil for Two-Dimensional Flow. Proc. Roy. Soc. of London, ser. A., vol. 111, pp. 592-603, June 2, 1926.

9. Zebb, Keirn: Technique of Measuring Transverse Components of Velocity Fluctuations in Turbulent Flow. CIT, A. E. Thesis, 1943.

10. Glauert, H.: The Characteristics of a Karman Vortex Street in a Channel of Finite Breadth. Proc. Roy. Soc. of London, ser. A, vol. 120, pp. 34-46, Aug. 1, 1928.

11. Fage, A., and Johansen, F. C.: On the Flow of Air Behind an Inclined Flat Plate of Infinite Span. British ARC R and M 1104, 1927.

12. Dryden, H. L., Schubauer, G. B., Mock, W. C., Jr., and Skramstad, H. K.: Measurements of Intensity and Scale of Wind-Tunnel Turbulence and Their Relation to the Critical Reynolds Number of Spheres. NACA Rep. 581, 1937.

13. Liepmann, H. W.: Aspects of the Turbulence Problem. Jour. Appl. Math. Phy. (ZAMP), vol. 3, fasc. 5 and 6, pp. 321-342; 407-426, 1952.

14. Lamb, Sir Horace: Hydrodynamics. Dover Publications, p. 224, 1945.

15. Roshko, A.: On the Wake and Drag of Bluff Bodies. Jour. Aero. Sci., vol. 22, no. 2, pp. 124-132, Feb. 1955.

16. Hollingdale, S. H.: Stability and Configuration of the Wakes Produced by Solid Bodies Moving through Fluids. Phil. Mag., 7th series, vol. 29, pt. 1, pp. 209-257, Mar. 1940.

17. Dryden, H. L.: Turbulence Investigation at the National Bureau of Standards. Proc. Fifth Int. Cong. Appl. Mech. (Sept. 1938, Cambridge, Mass.), John Wiley and Sons, Inc., pp. 362-368, 1939.

18. Batchelor, G. K.: The Theory of Homogeneous Turbulence. Cambridge Univ. Press, pp. 45-47, 1953.

19. Summers, J. L., and Page, W. A.: Lift and Moment Characteristics at Subsonic Mach Numbers of Four 10-Percent-Thick Airfoil Sections of Varying Trailing-Edge Thickness. NACA RM A50J09, 1950.

20. Goldstein, S., ed.: Modern Developments in Fluid Dynamics. Oxford Univ. Press, vol. 2, p. 419, 1938.

21. Liepmann, H. W.: Extension of the Statistical Approach to Buffeting and Gust Response of Wings of Finite Span. Jour. Aero. Sci., vol. 22, no. 3, pp. 197-200, March 1955.

22. Duncan, W. J., Ellis, D. L., and Scruton, C.: Two Reports on Tail Buffeting (1st Report). British ARC R and M 1457, 1932.

23. Ferri, Antonio: Preliminary Investigation of Downwash Fluctuations of a High-Aspect-Ratio Wing in the Langley 8-Foot High-Speed Tunnel. NACA RM L6H28b, 1946.

24. Sorenson, R. M., Wyss, J. A., and Kyle, J. C.: Preliminary Investigation of the Pressure Fluctuations in the Wakes of Two-Dimensional Wings at Low Angles of Attack. NACA RM A51G10, 1951.

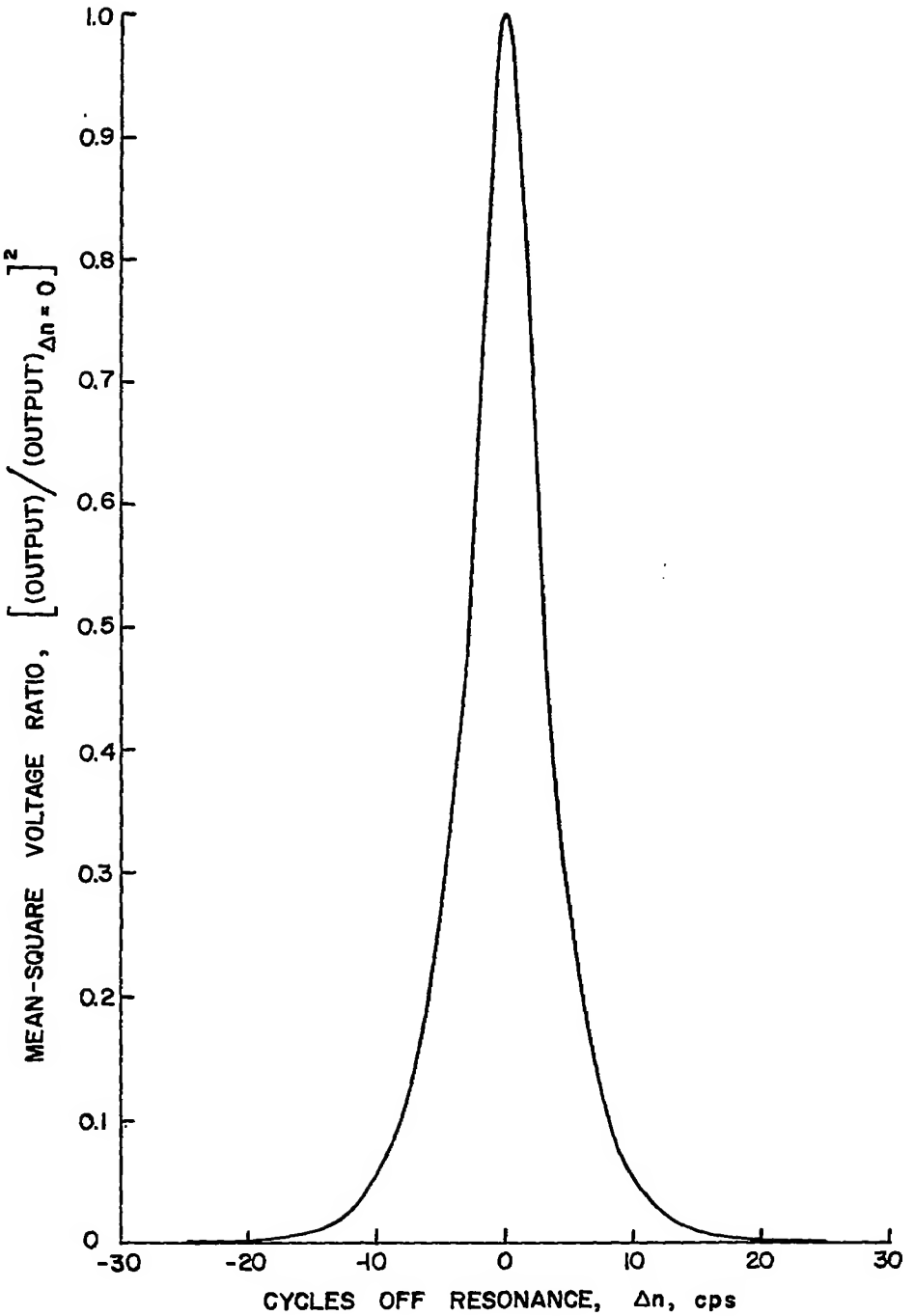

Figure 1.- Filtering characteristics of Hewlett-Packard model 300A wave analyzer for 30 cps half-band width.

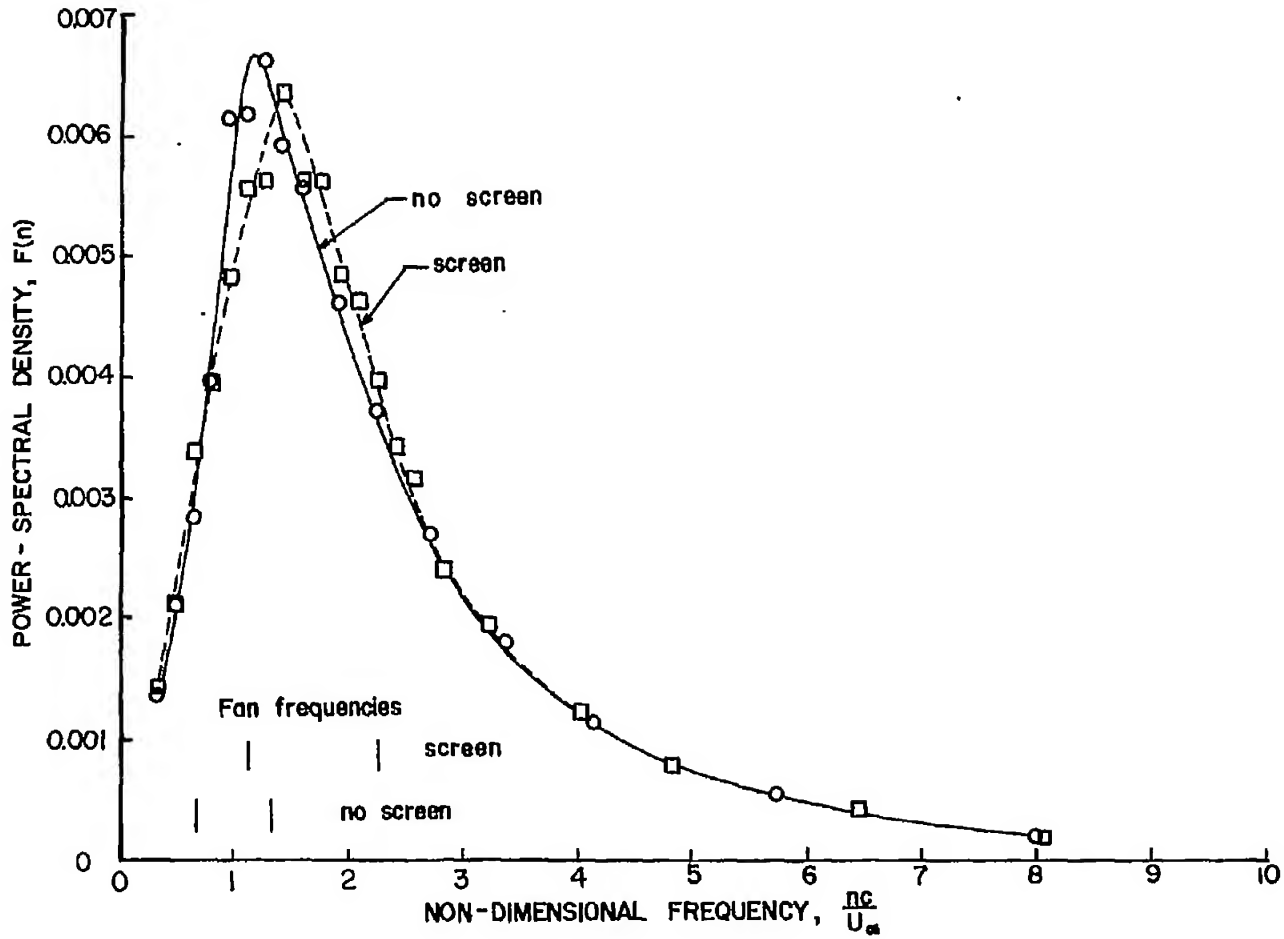

Figure 2.- Effect of tunnel fan frequency on measurement of w^2 power spectrum $\alpha = 6^{\circ}25'$, $U_\infty = 31$ fps, $x = 1c$, $z = 0$.

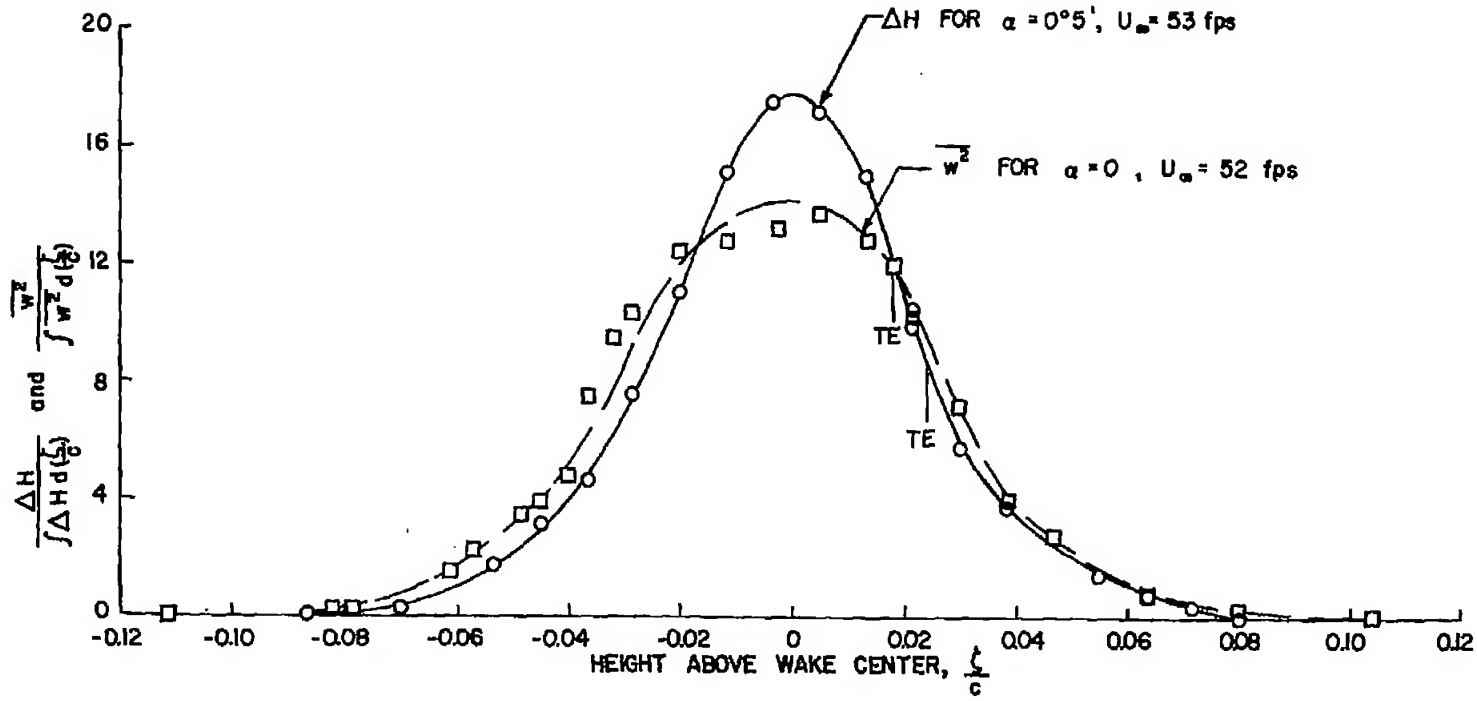

Figure 3.- Total-head and $\overline{w^2}$ profiles measured 1 chord length behind wing trailing edge at nominal zero incidence.

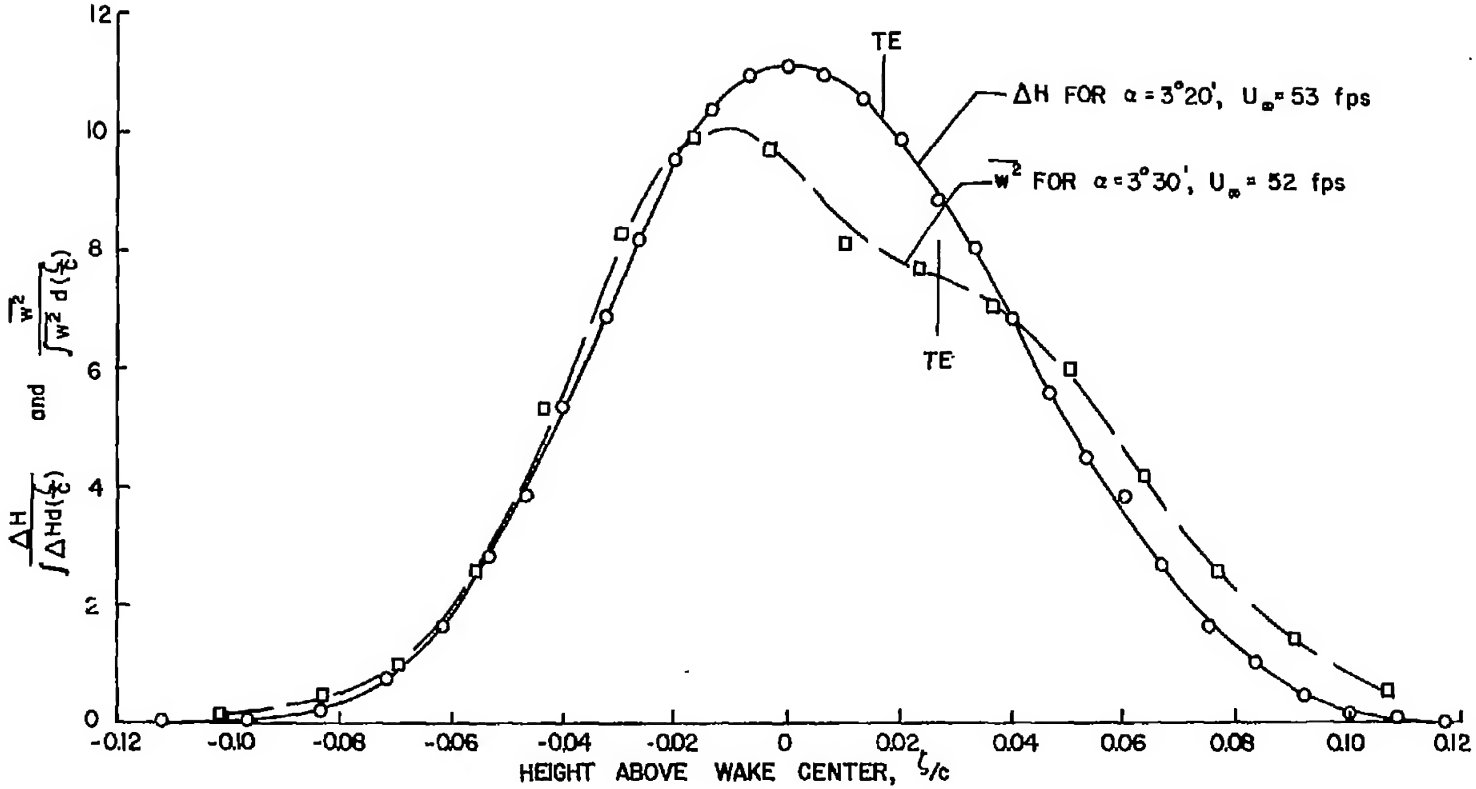

Figure 4.- Total-head and $\overline{w^2}$ profiles measured 1 chord length behind wing trailing edge at nominal incidence of 3 degrees.

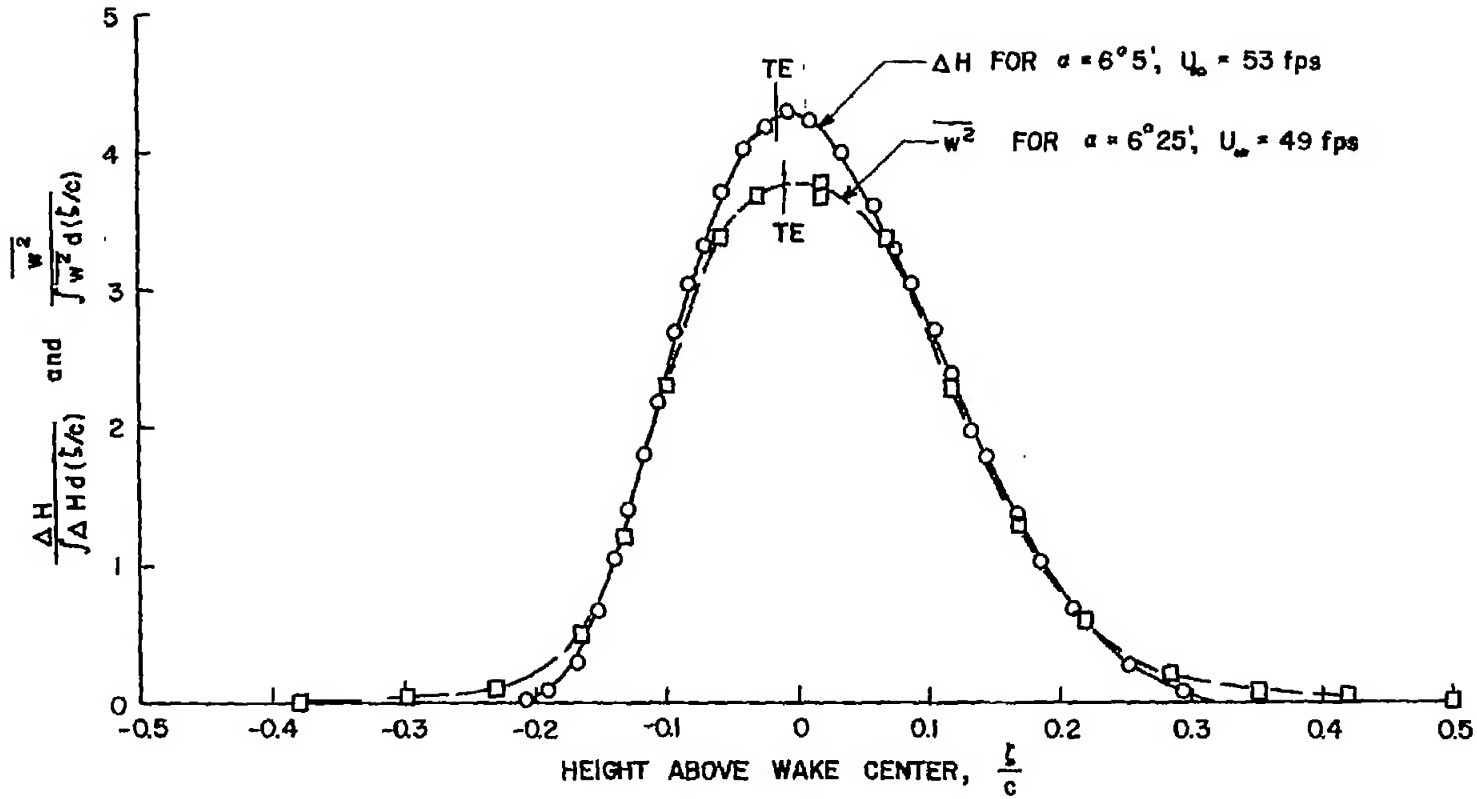

Figure 5.- Total-head and $\overline{w^2}$ profiles measured 1 chord length behind wing trailing edge at nominal incidence of 6 degrees.

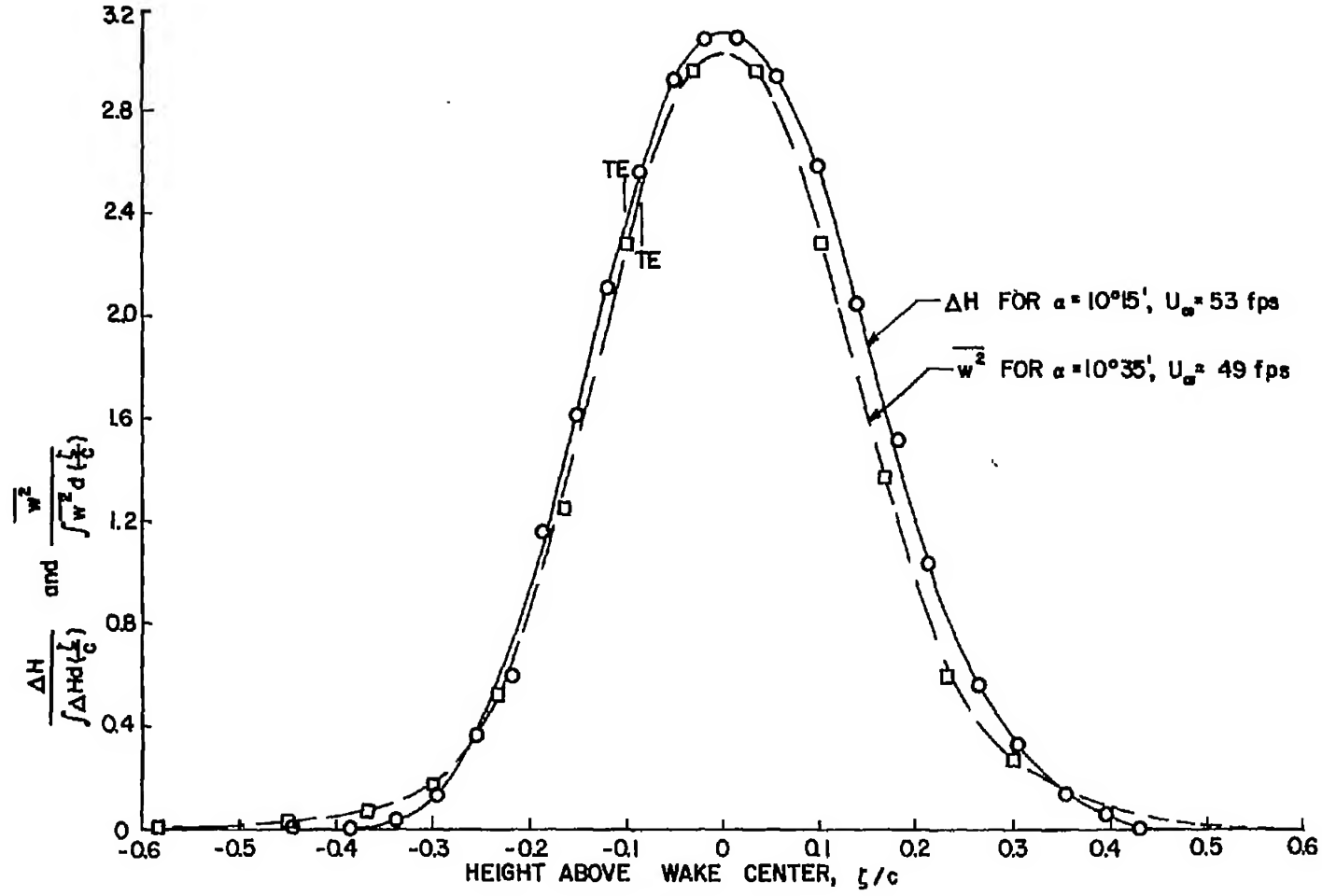

Figure 6.- Total-head and $\overline{w^2}$ profiles measured 1 chord length behind wing trailing edge at nominal incidence of 10 degrees.

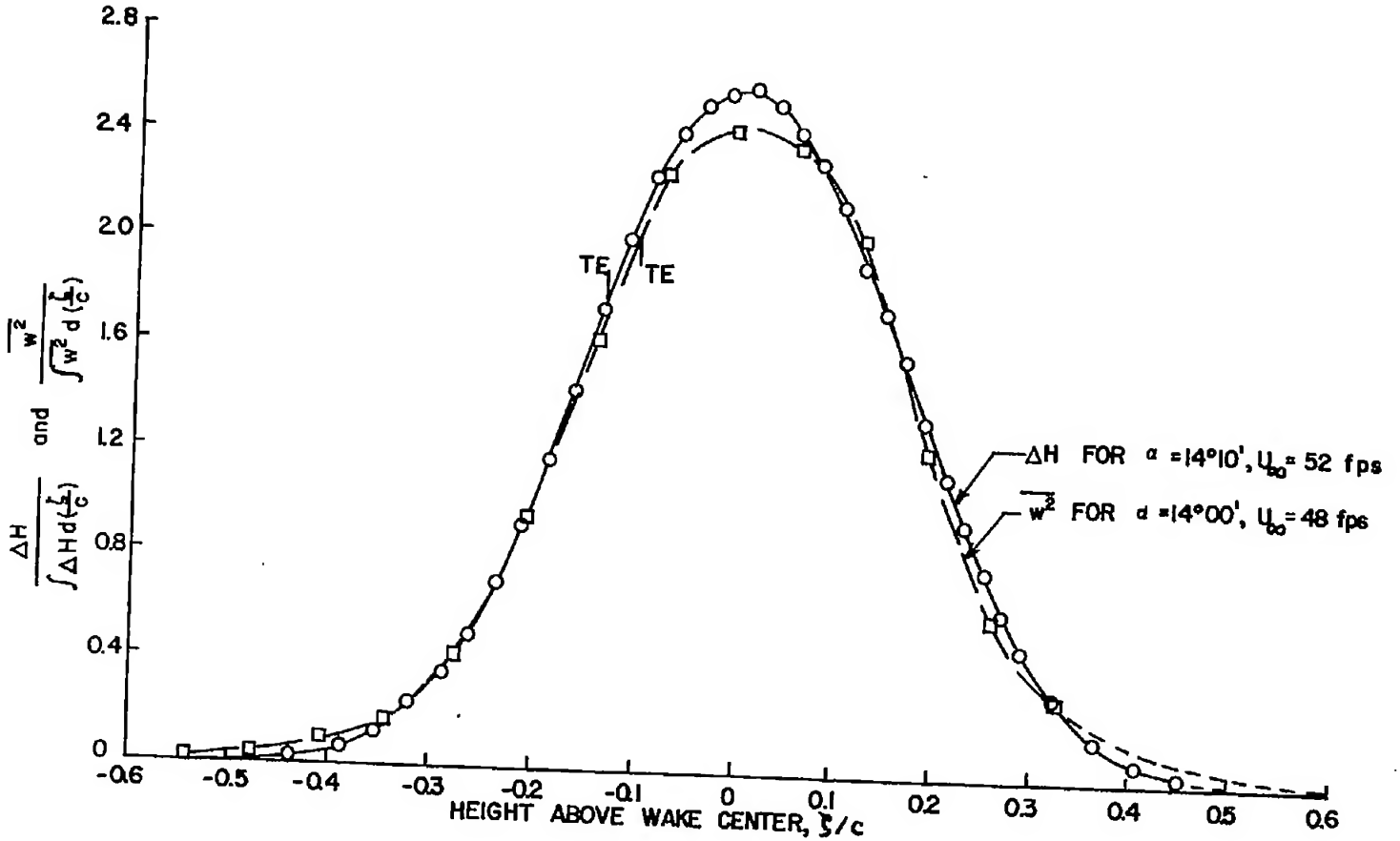

Figure 7.- Total-head and $\overline{w^2}$ profiles measured 1 chord length behind wing trailing edge at nominal incidence of 14 degrees.

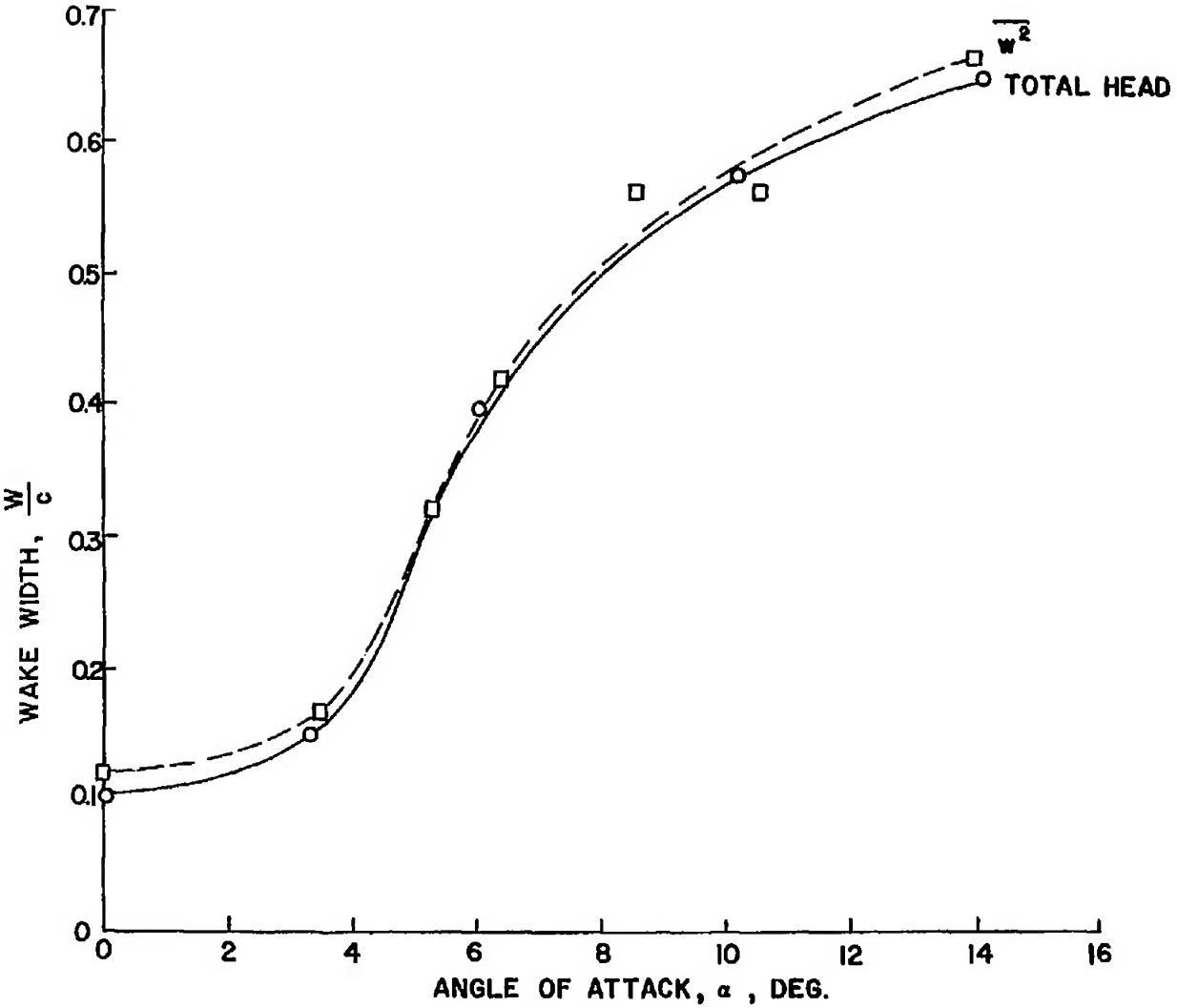

Figure 8.- Comparison of wake widths obtained from total-head and $\overline{w^2}$ measurements; x = 1c, U_∞ = 50 fps (nominal).

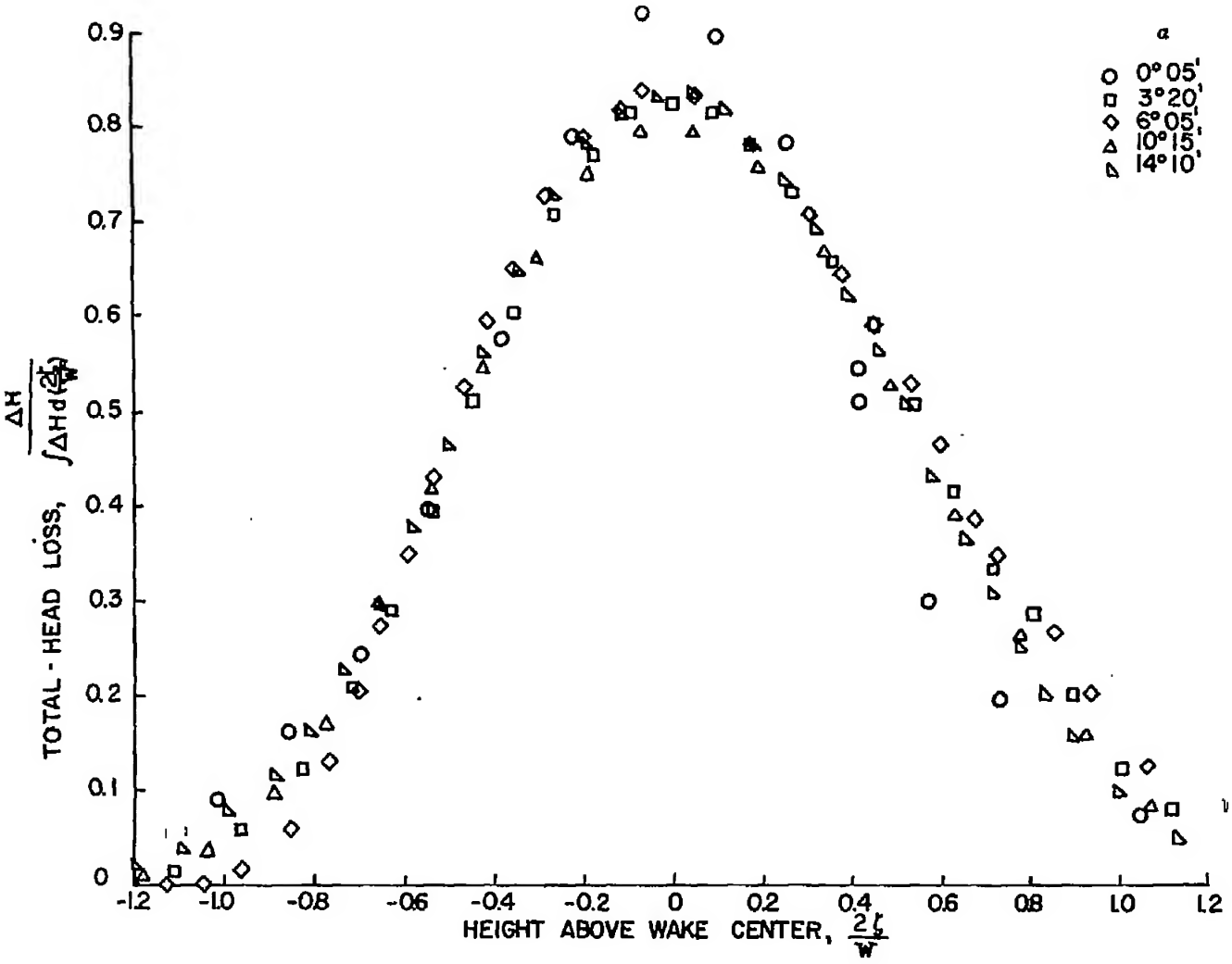

Figure 9.- Comparison of total-head profiles for several angles of attack; x = 1c, U_∞ = 53 fps (nominal).

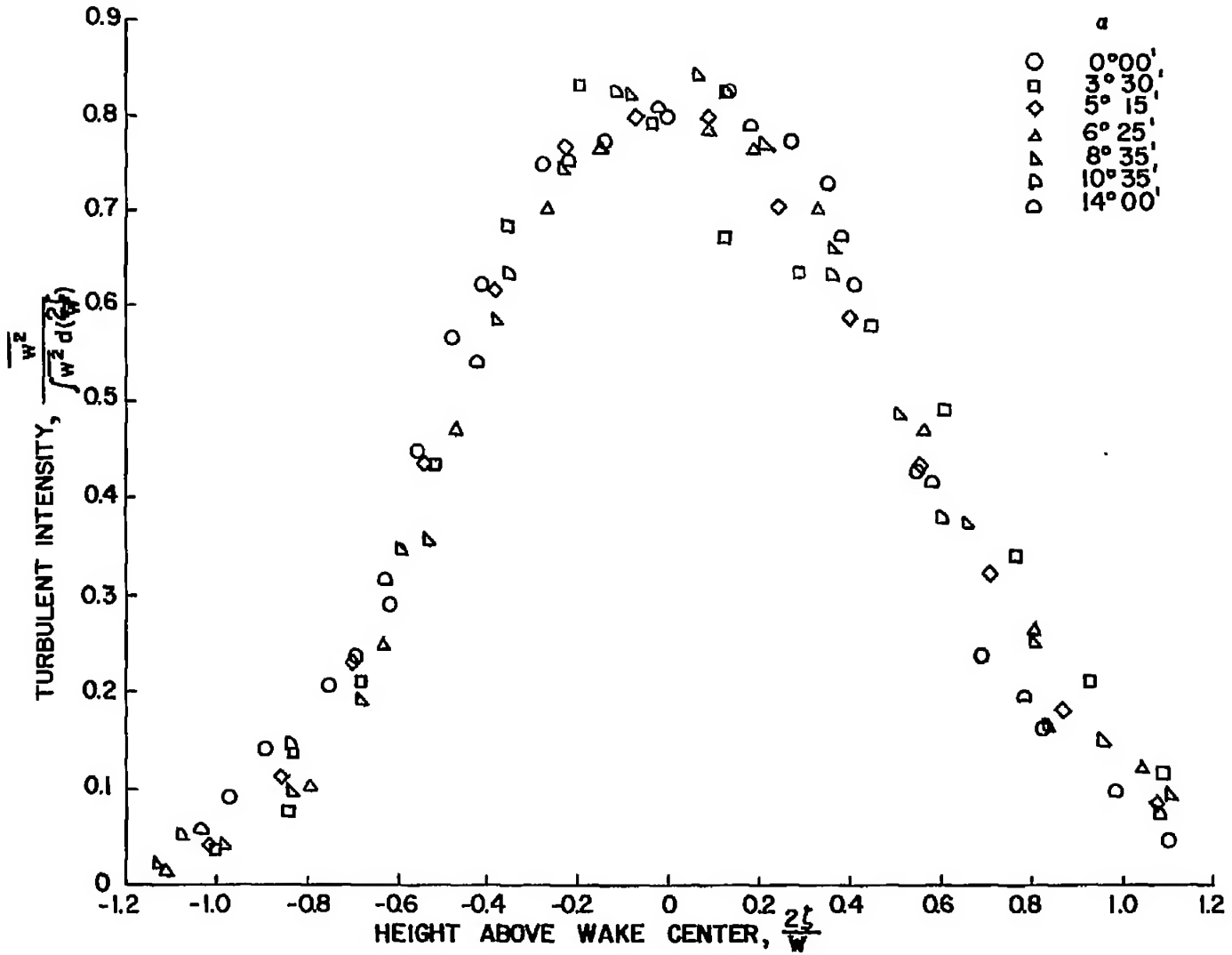

Figure 10.- Comparison of $\overline{w^2}$ profiles for several angles of attack; x = 1c, U_∞ = 50 fps (nominal).

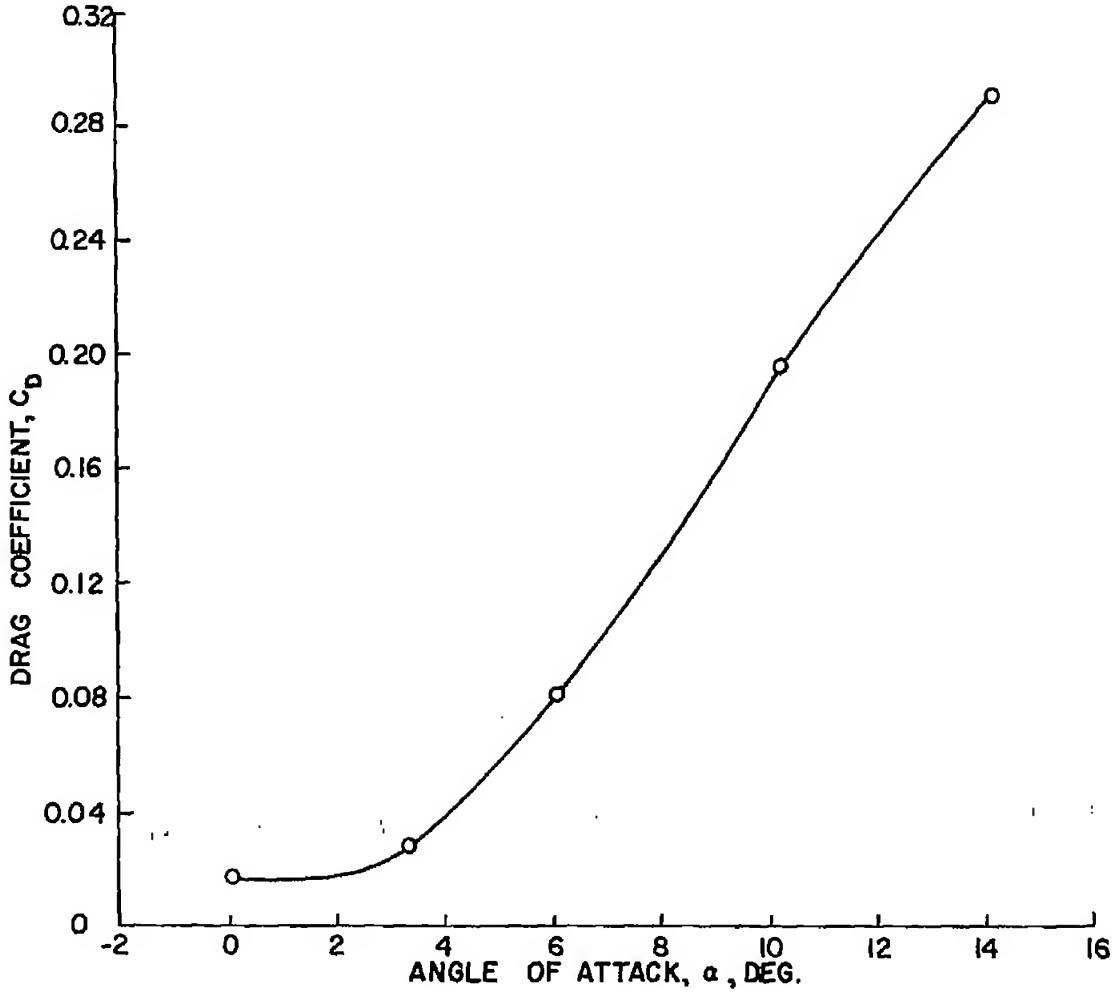

Figure 11.- Variation of wing drag coefficient with angle of attack; U_∞ = 53 fps (nominal).

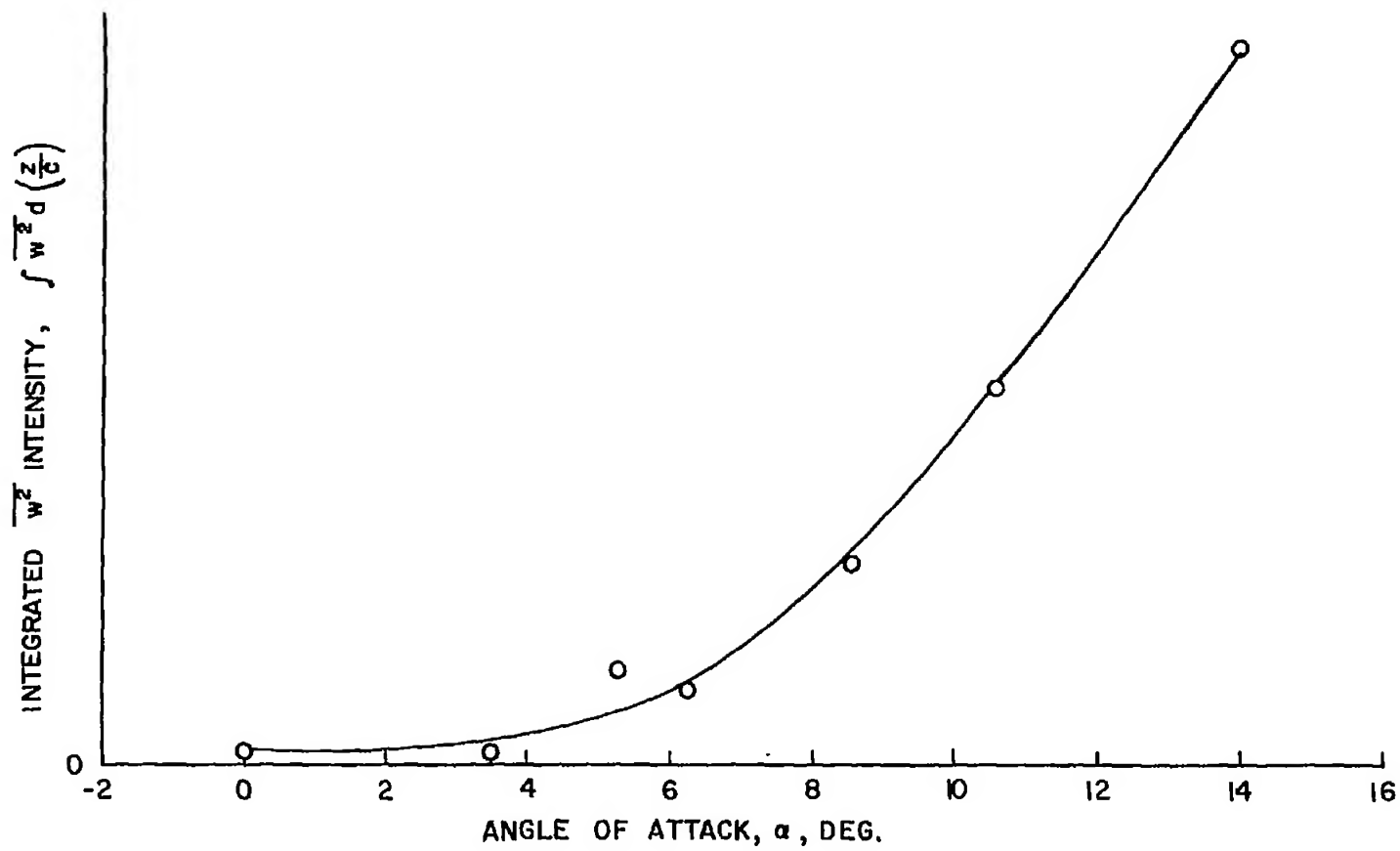

Figure 12.- Variation of integrated $\overline{w^2}$ intensity with angle of attack, $x = 1c$, $U_\infty = 50$ fps (nominal).

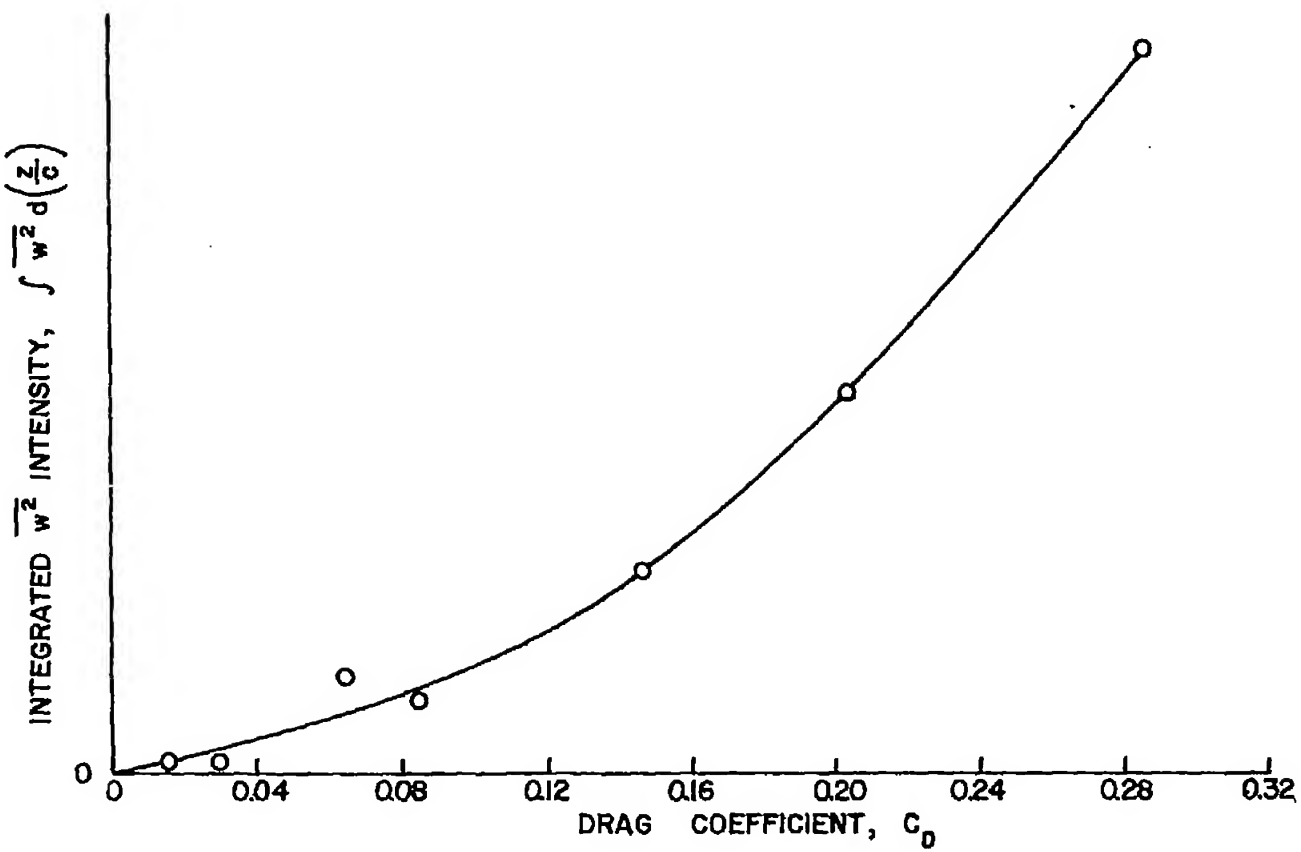

Figure 13.- Variation of integrated $\overline{w^2}$ intensity with drag coefficient; x = 1c, U_∞ = 50 fps (nominal).

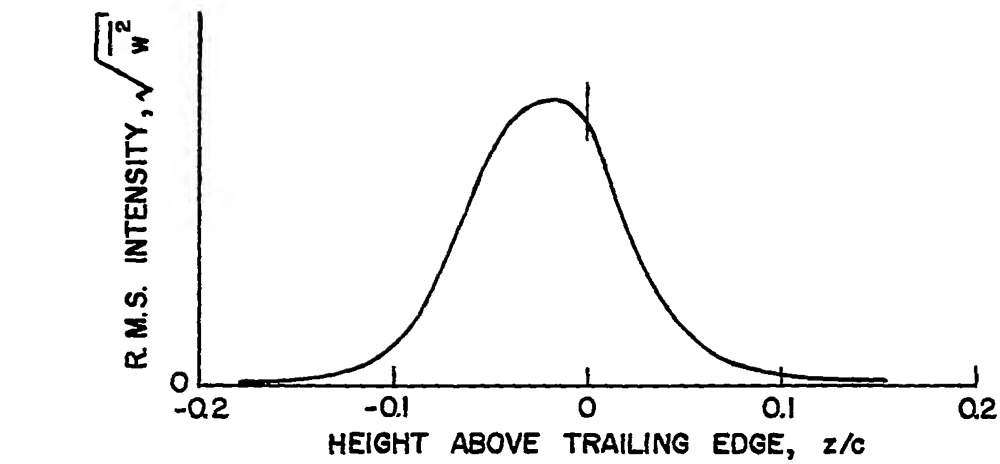

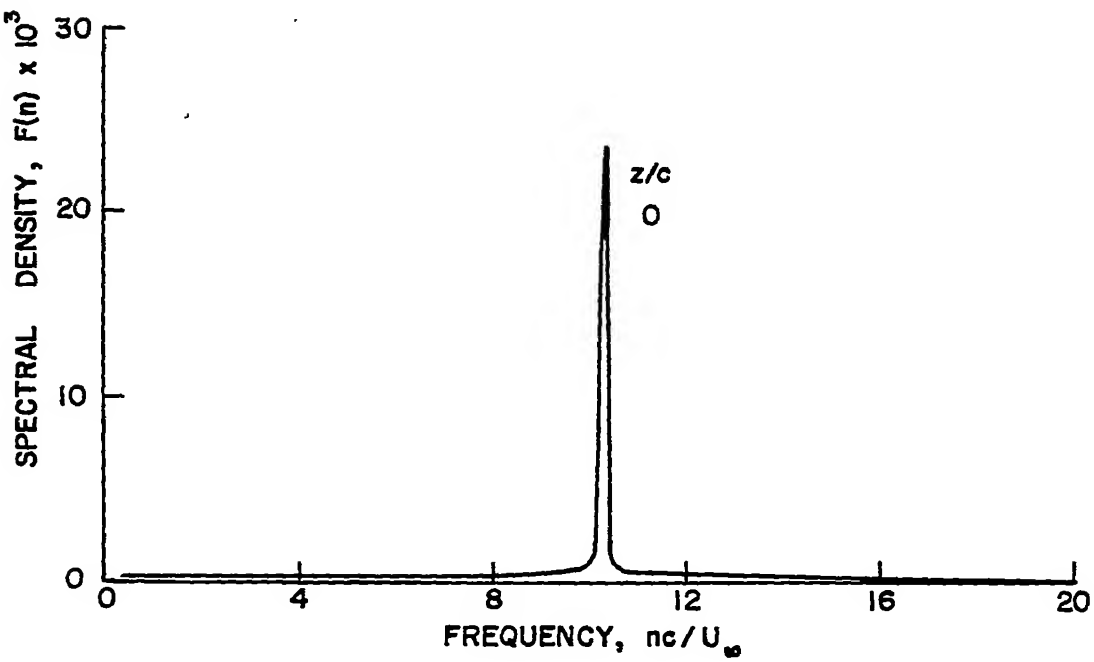

Figure 14.- RMS downwash intensity and w^2 power spectrum measured 1 chord length behind trailing edge; $\alpha = 0$; $U_\infty = 52$ fps.

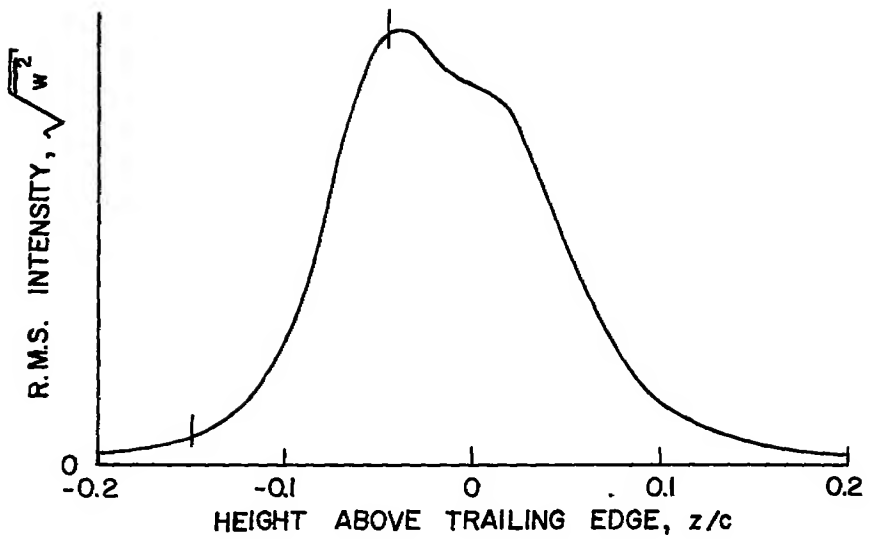

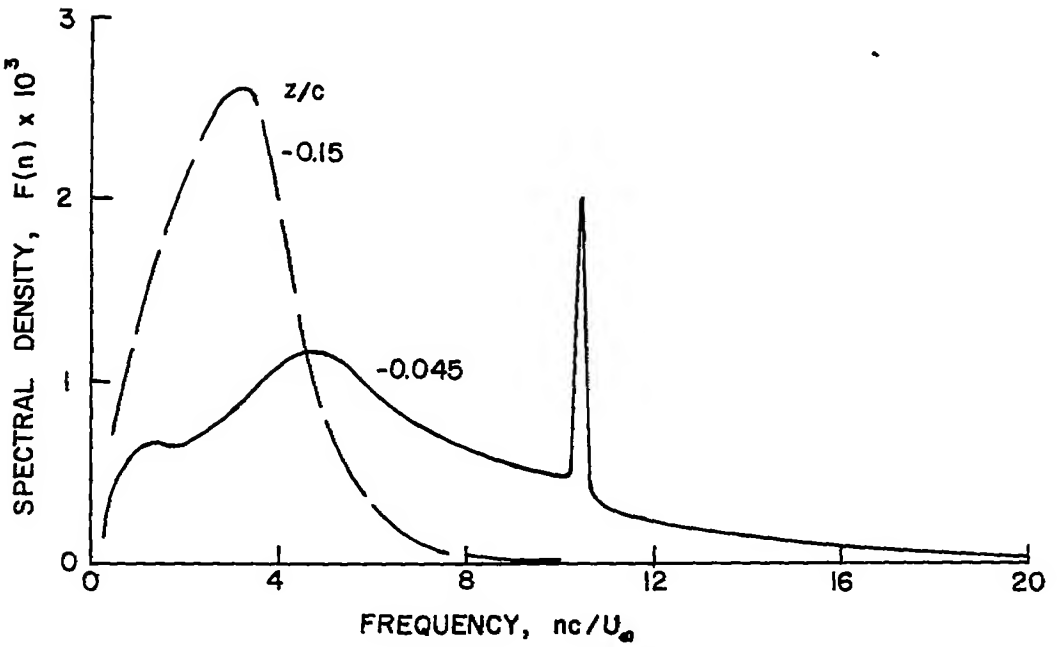

Figure 15.- RMS downwash intensity and w^2 power spectrum measured 1 chord length behind trailing edge; $\alpha = 3^\circ30'$, $U_\infty = 52$ fps.

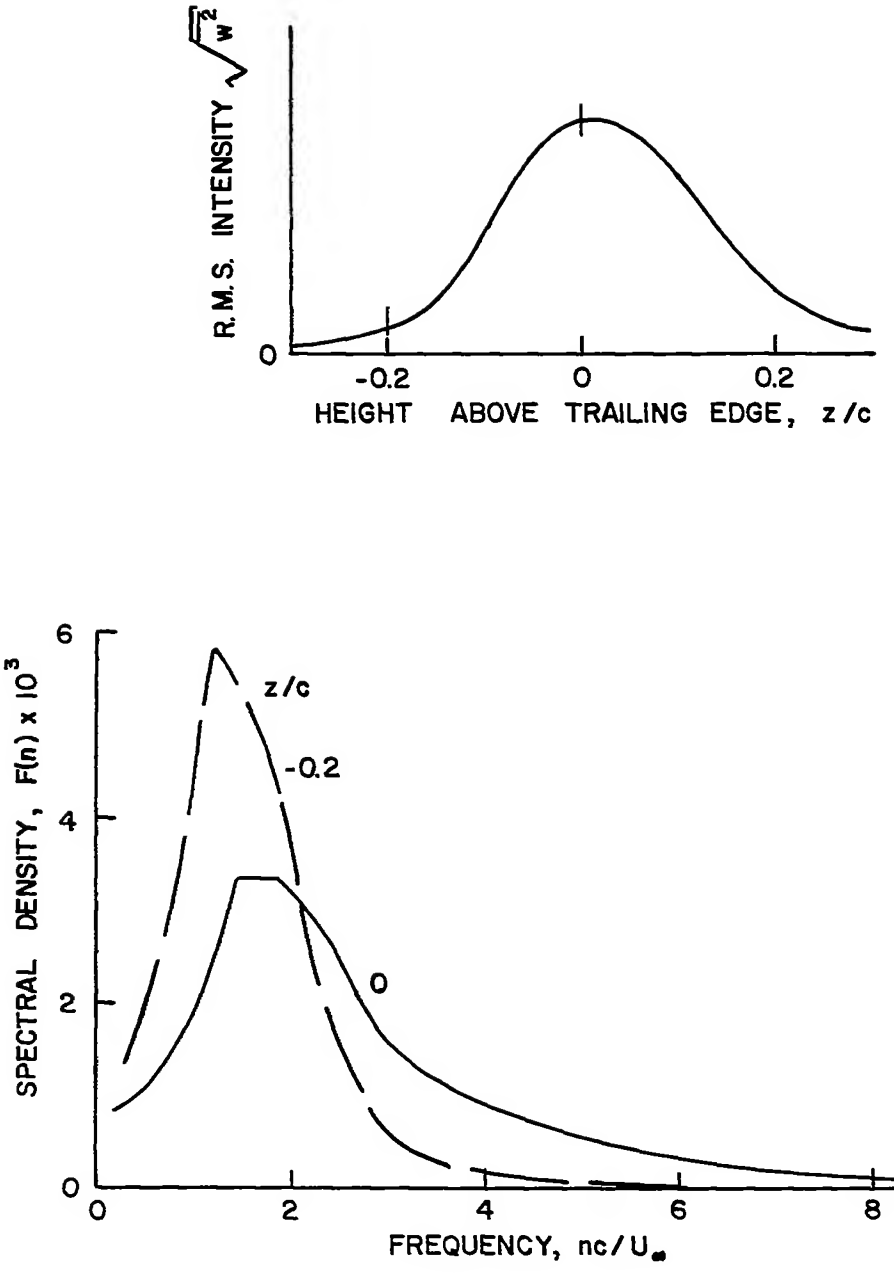

Figure 16.- RMS downwash intensity and w^2 power spectrum measured 1 chord length behind trailing edge; $\alpha = 5^\circ 15'$, $U_\infty = 52$ fps.

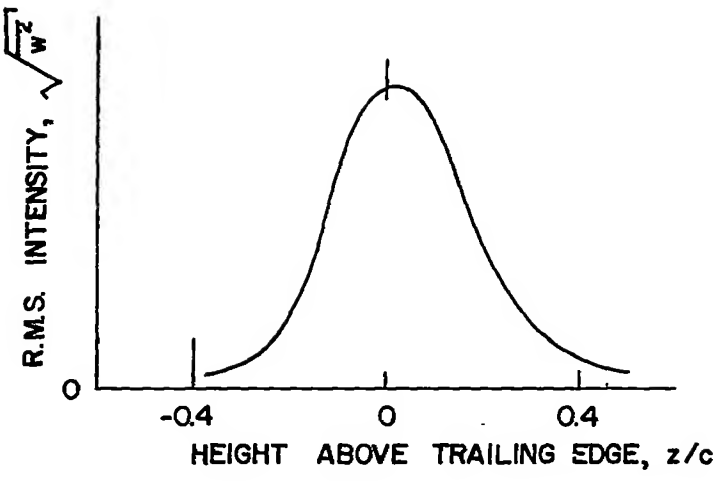

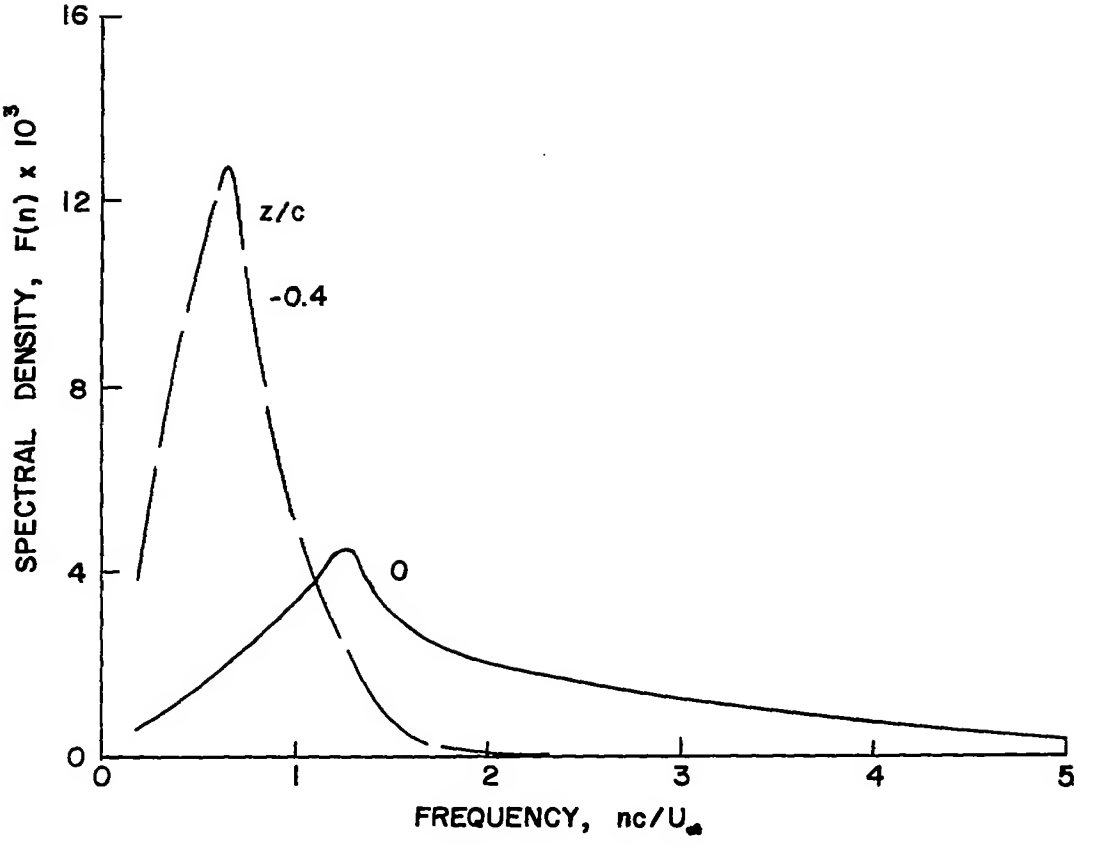

Figure 17.- RMS downwash intensity and $\overline{w^2}$ power spectrum measured 1 chord length behind trailing edge; $\alpha = 6°20'$, $U_\infty = 54$ fps.

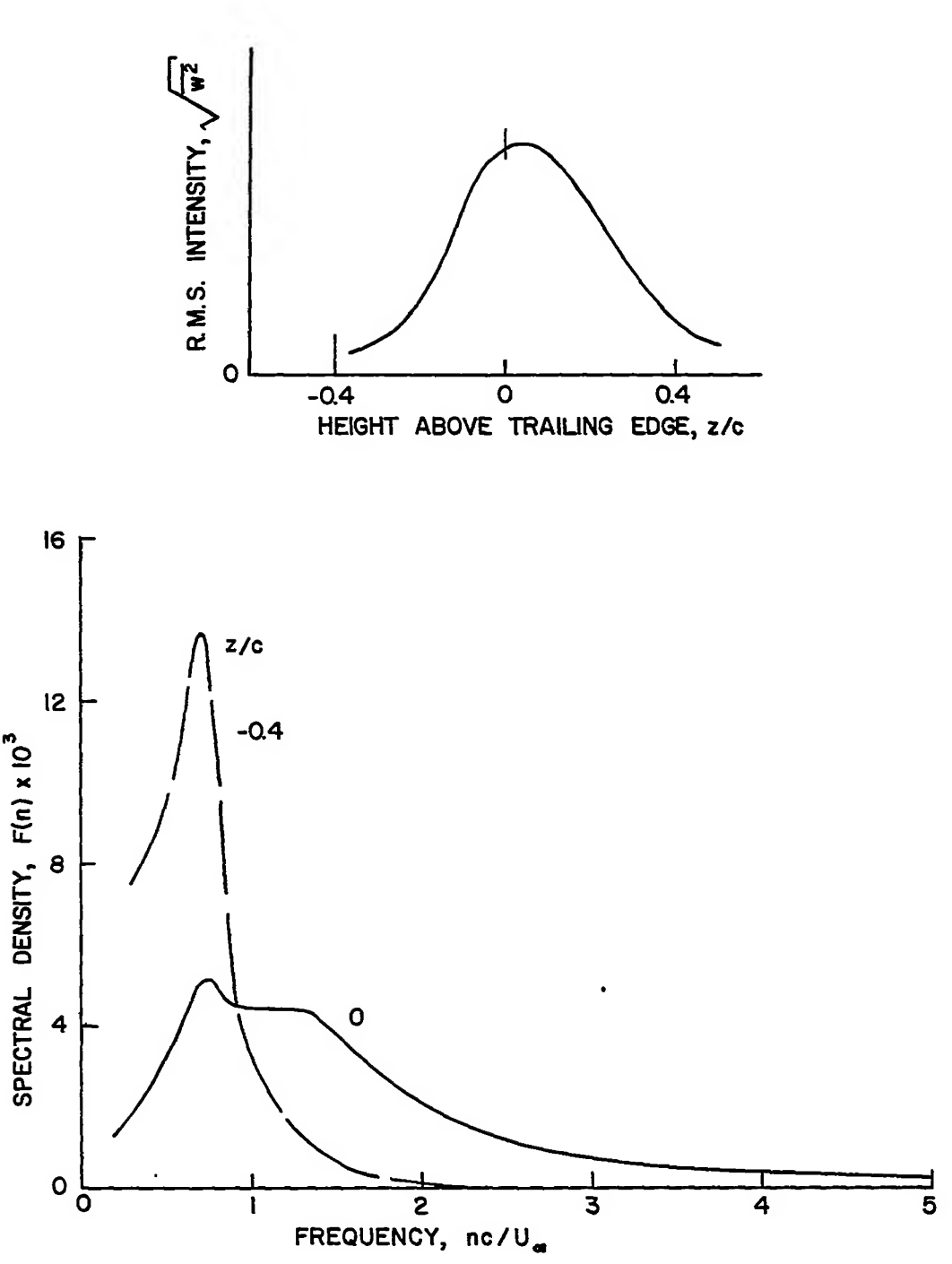

Figure 18.- RMS downwash intensity and w^2 power spectrum measured 1 chord length behind trailing edge; $\alpha = 8^\circ 35'$, $U_\infty = 52$ fps.

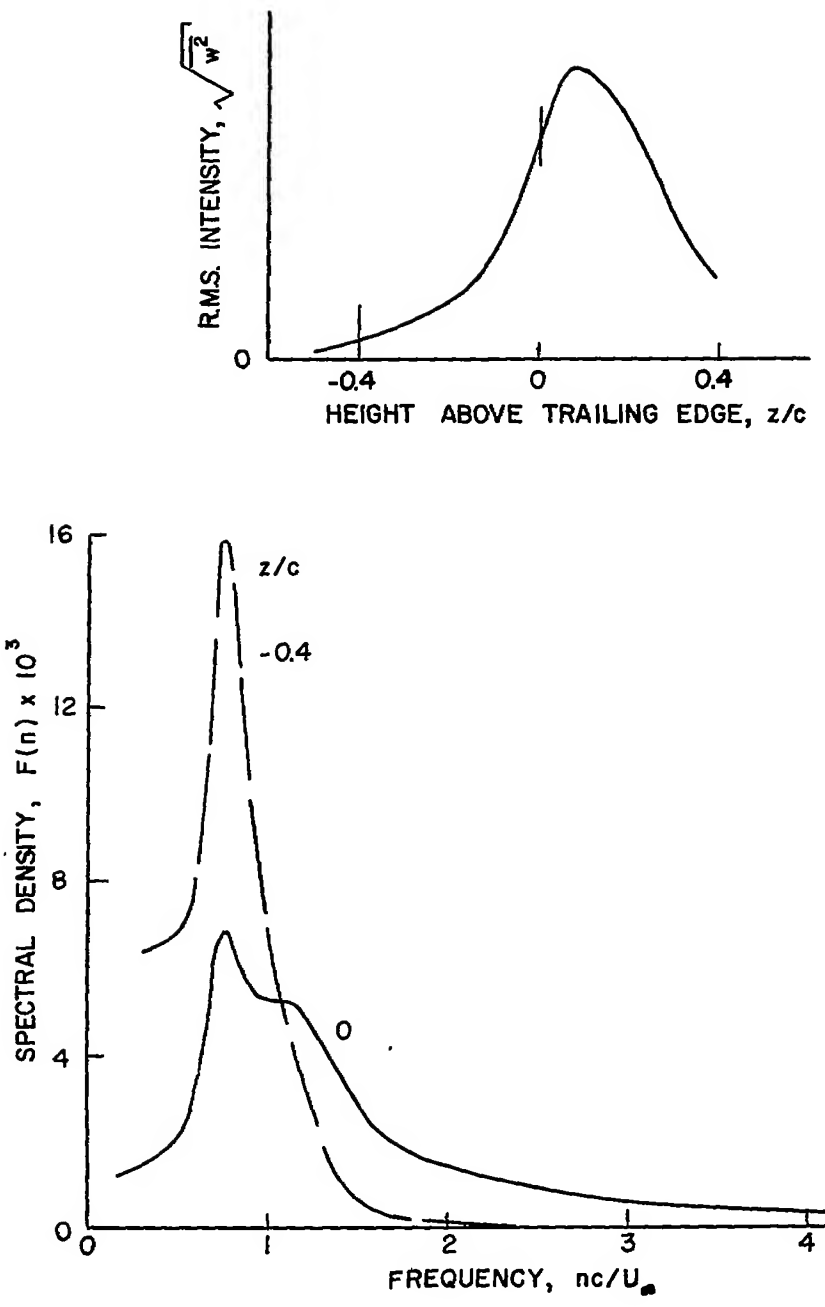

Figure 19.- RMS downwash intensity and w^2 power spectrum measured 1 chord length behind trailing edge; $\alpha = 10^\circ 15'$, $U_\infty = 57$ fps for $z = 0$; $\alpha = 10^\circ 35'$, $U_\infty = 48$ fps for $z/c = -0.4$.

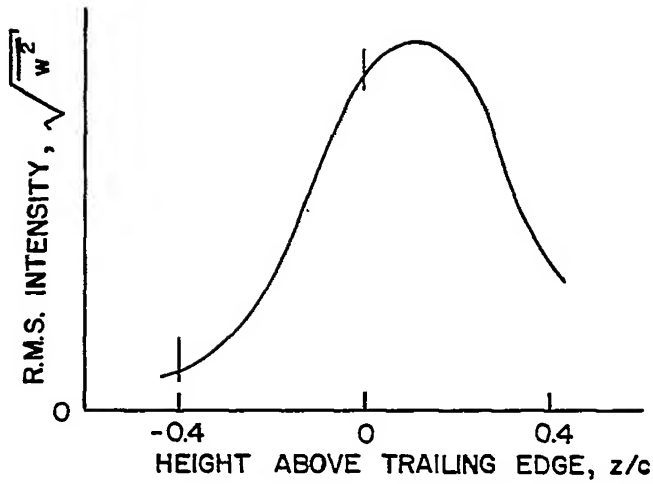

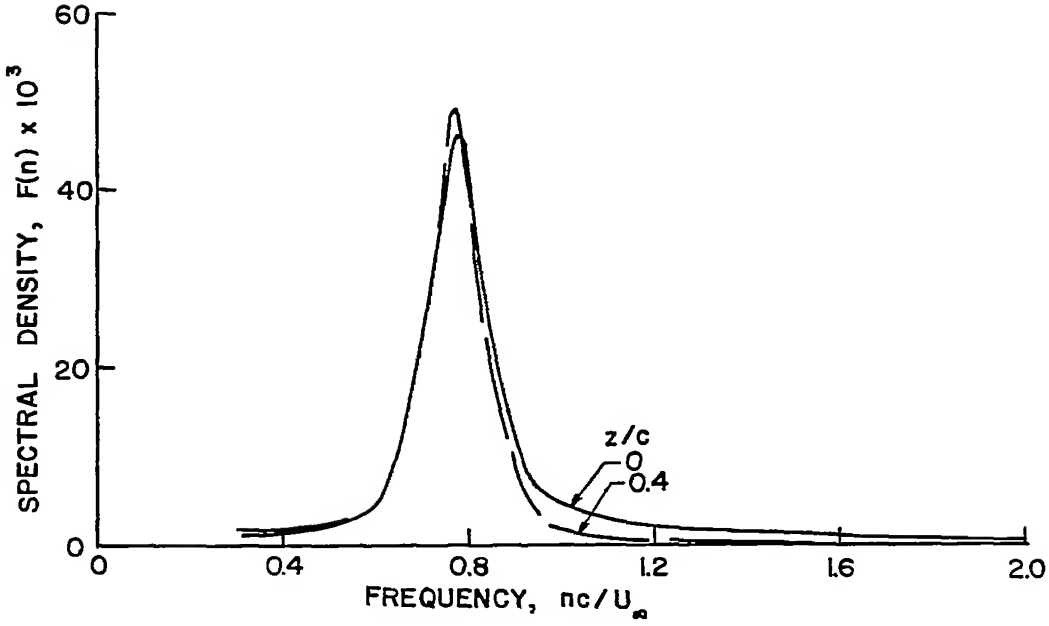

Figure 20.- RMS downwash intensity and w^2 power spectrum measured 1 chord length behind trailing edge; $\alpha = 14^\circ$, $U_\infty = 48$ fps for $z = 0$, $U_\infty = 52$ fps for $z/c = -0.4$.

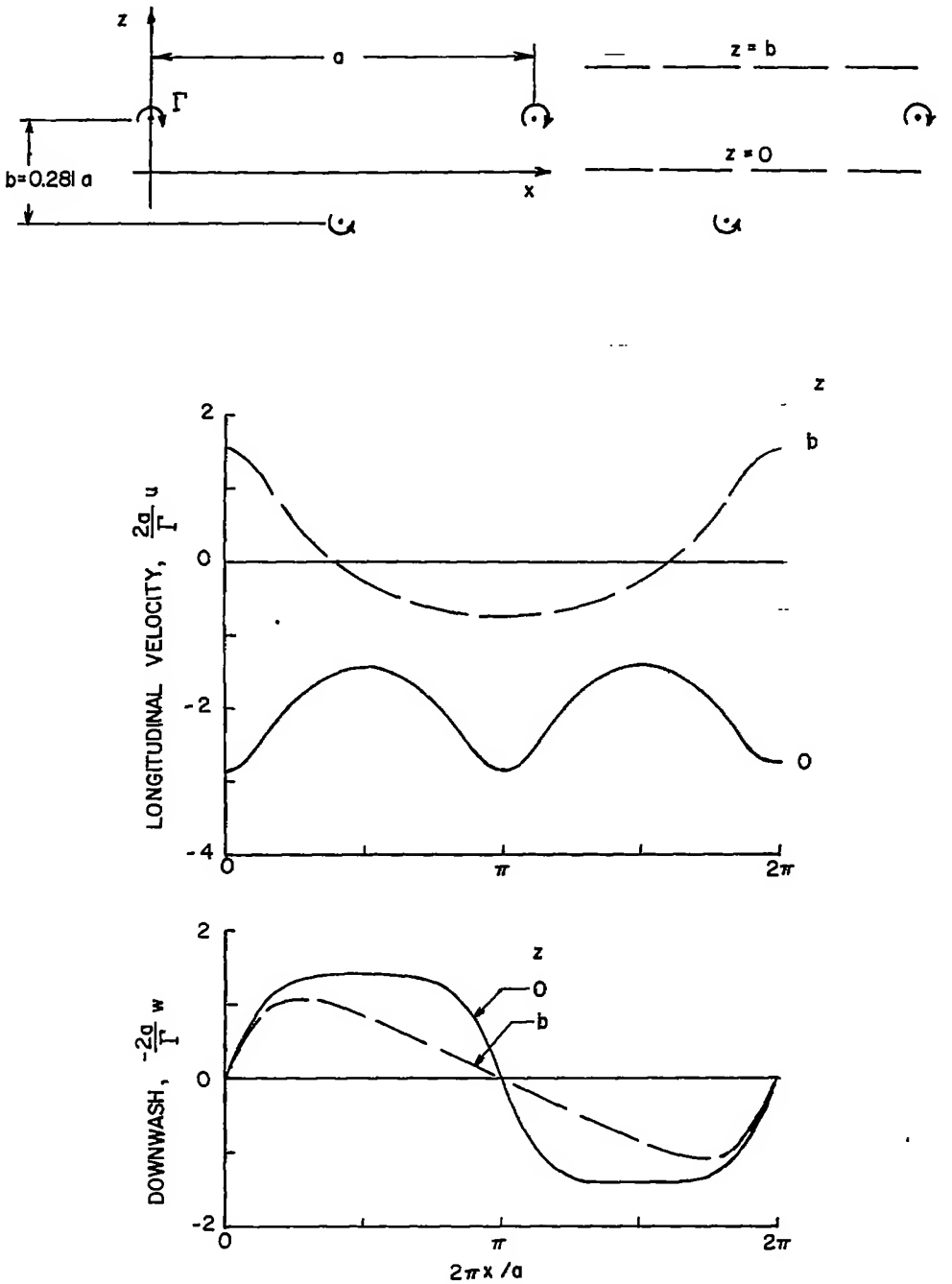

Figure 21.- The velocities induced by a vortex street.

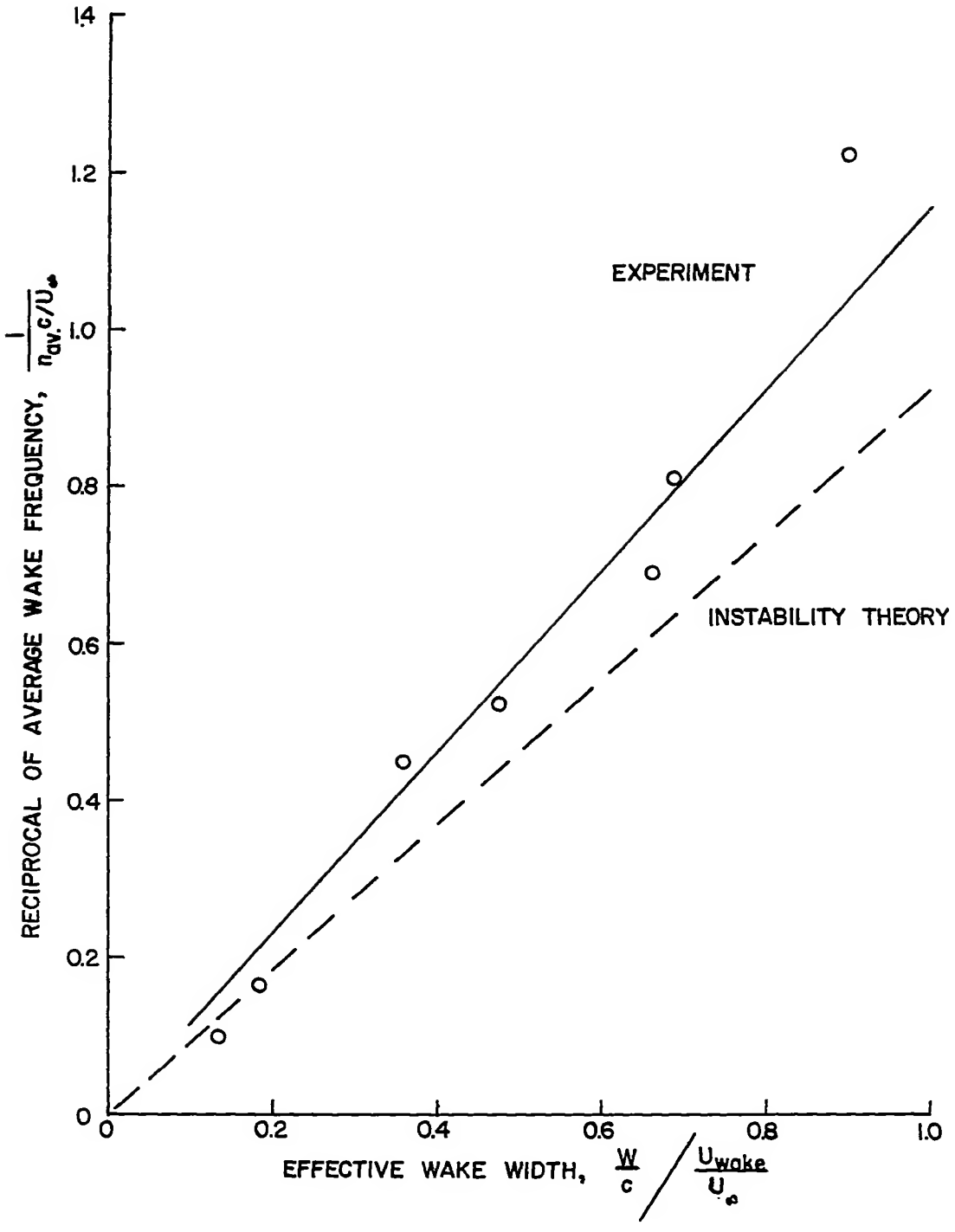

Figure 22.- Dependence of average wake frequency on effective wake width.

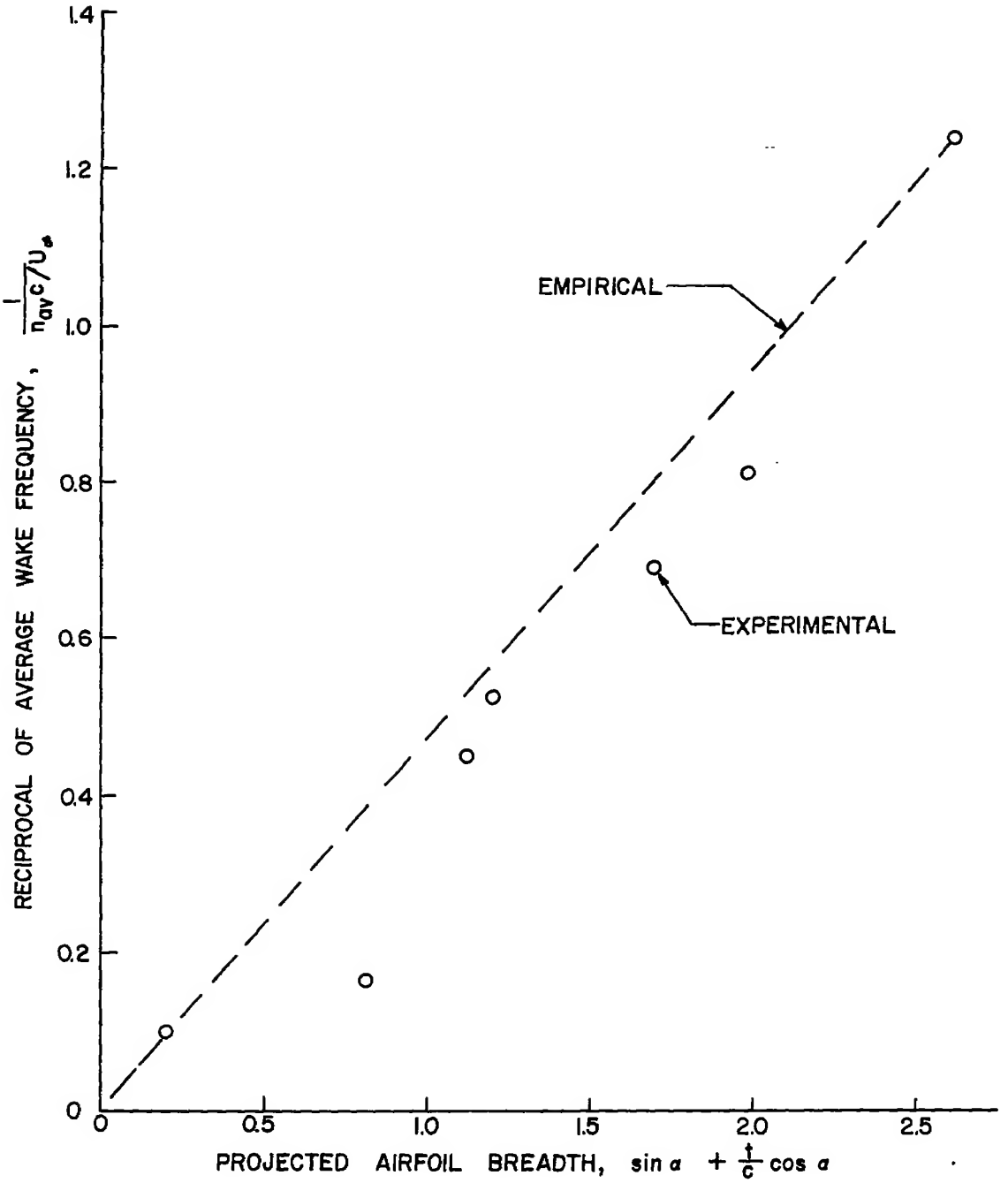

Figure 23.- Dependence of average wake frequency on projected airfoil breadth.

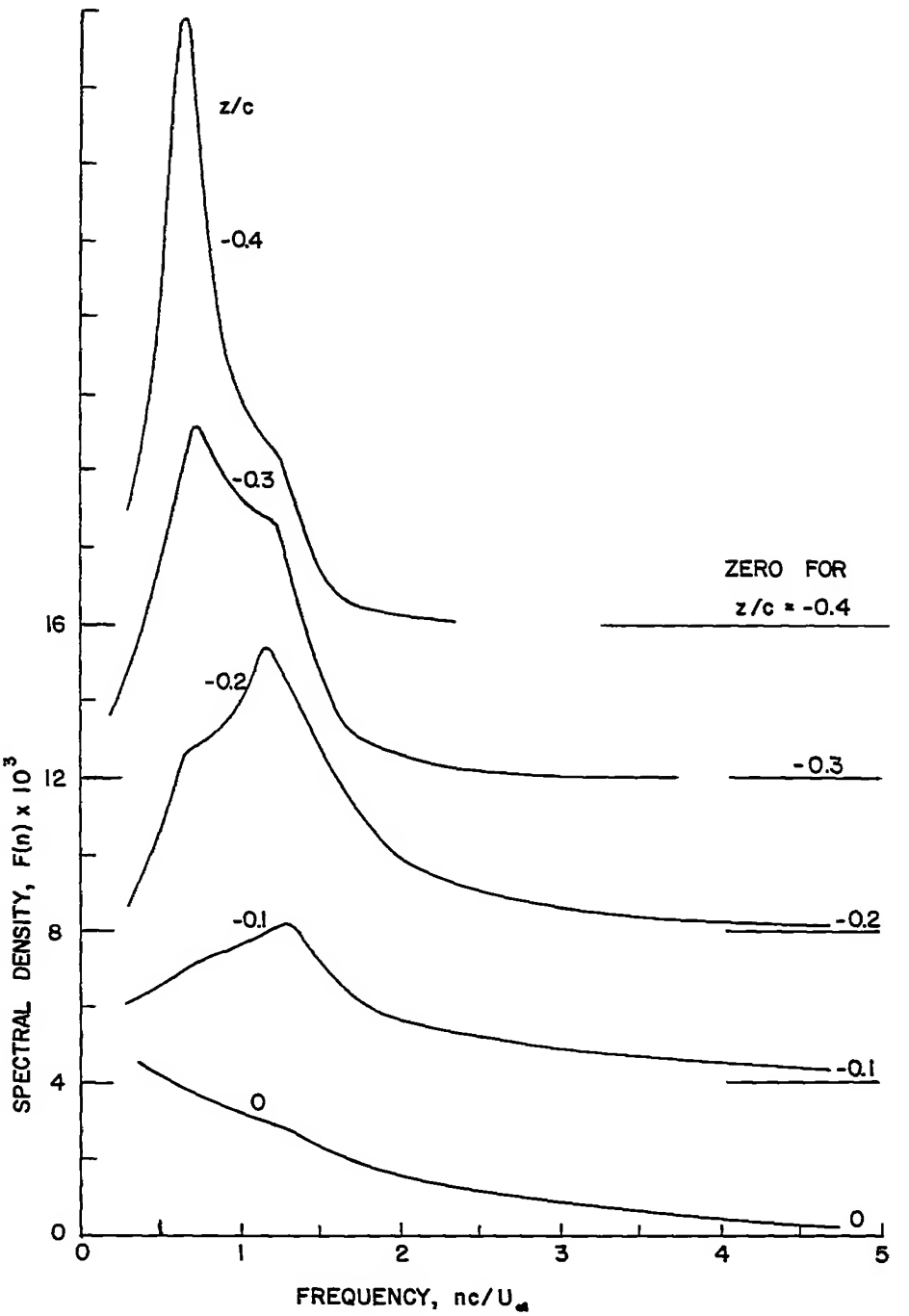

Figure 24.- u^2 power spectrum; $\alpha = 6°20'$, $U_\infty = 54$ fps, $x = 1c$.

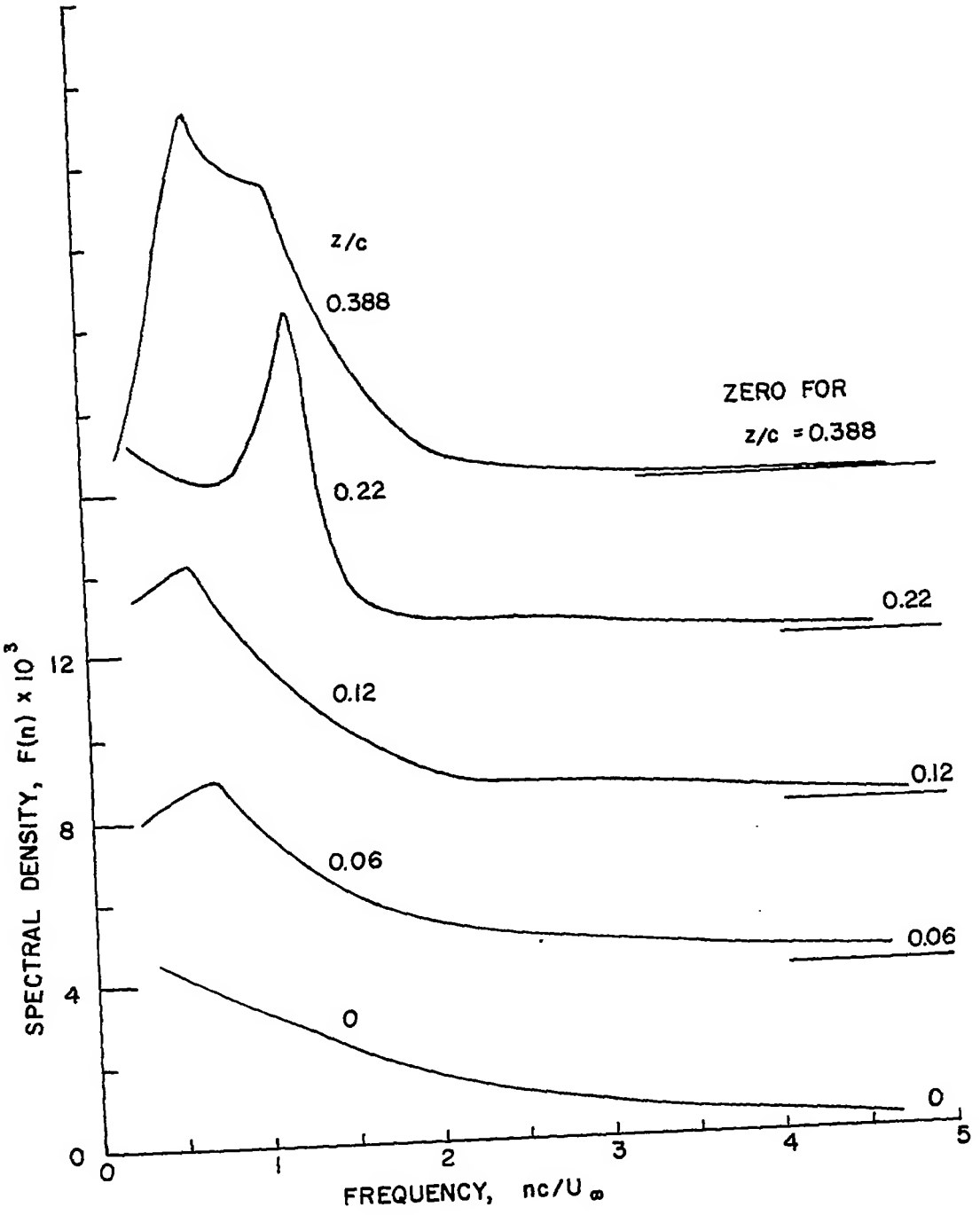

Figure 25.- u^2 power spectrum; $\alpha = 6°20'$, $U_\infty = 54$ fps, $x = 1c$.

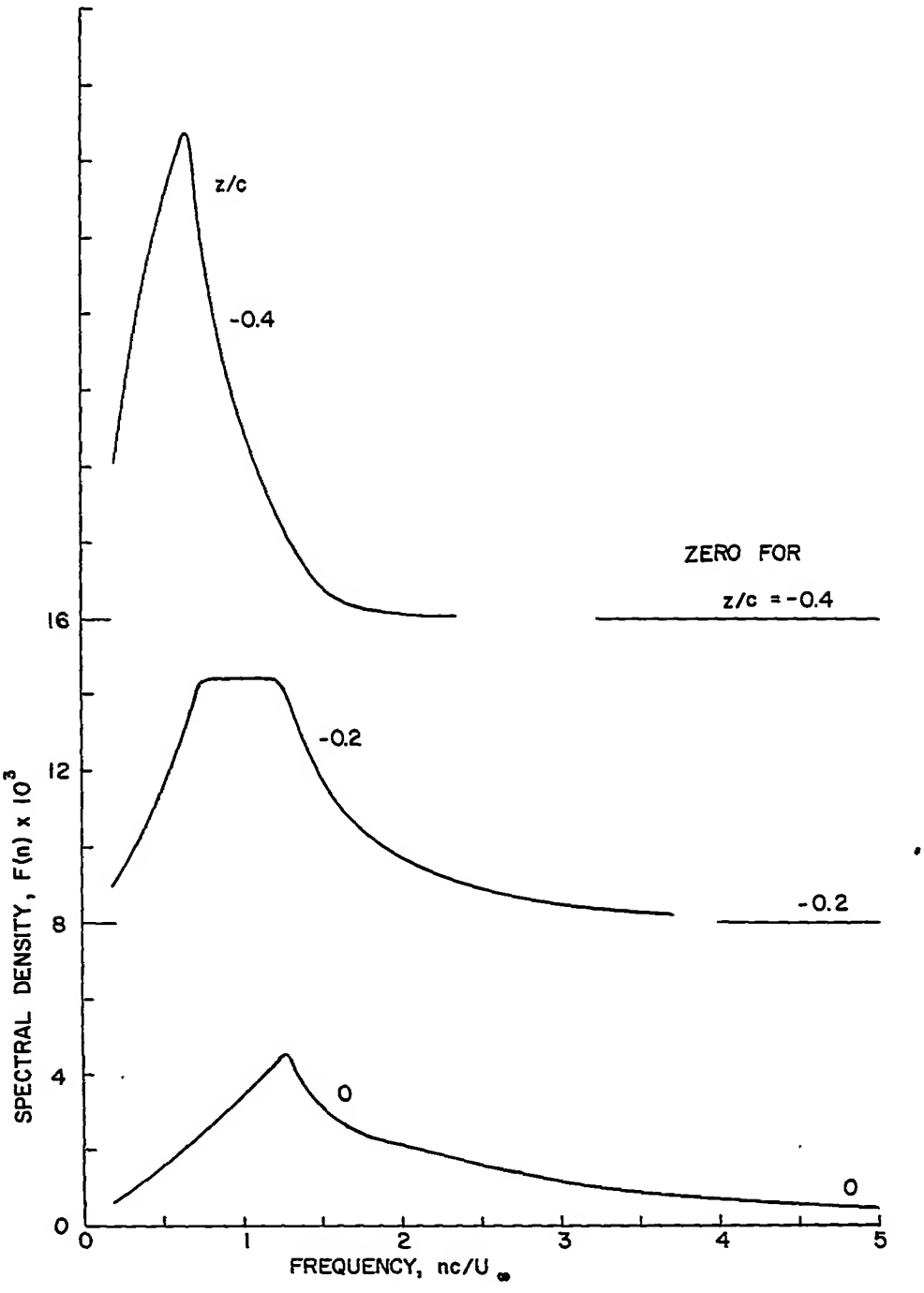

Figure 26.- w^2 power spectrum; $\alpha = 6^{\circ}20'$, $U_{\infty} = 54$ fps, $x = 1c$.

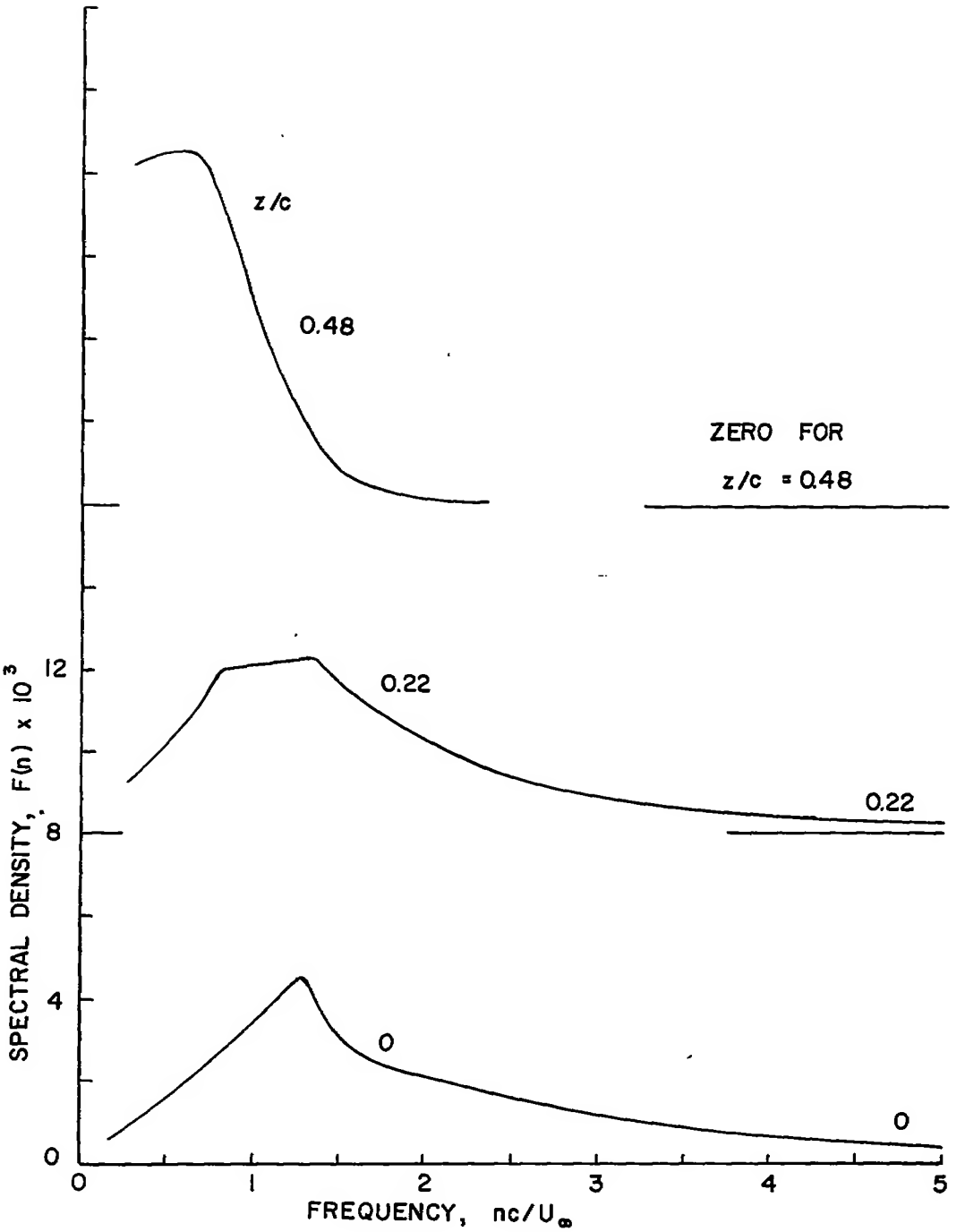

Figure 27.- w^2 power spectrum; $\alpha = 6^{\circ}20'$, $U_{\infty} = 54$ fps, $x = 1c$.

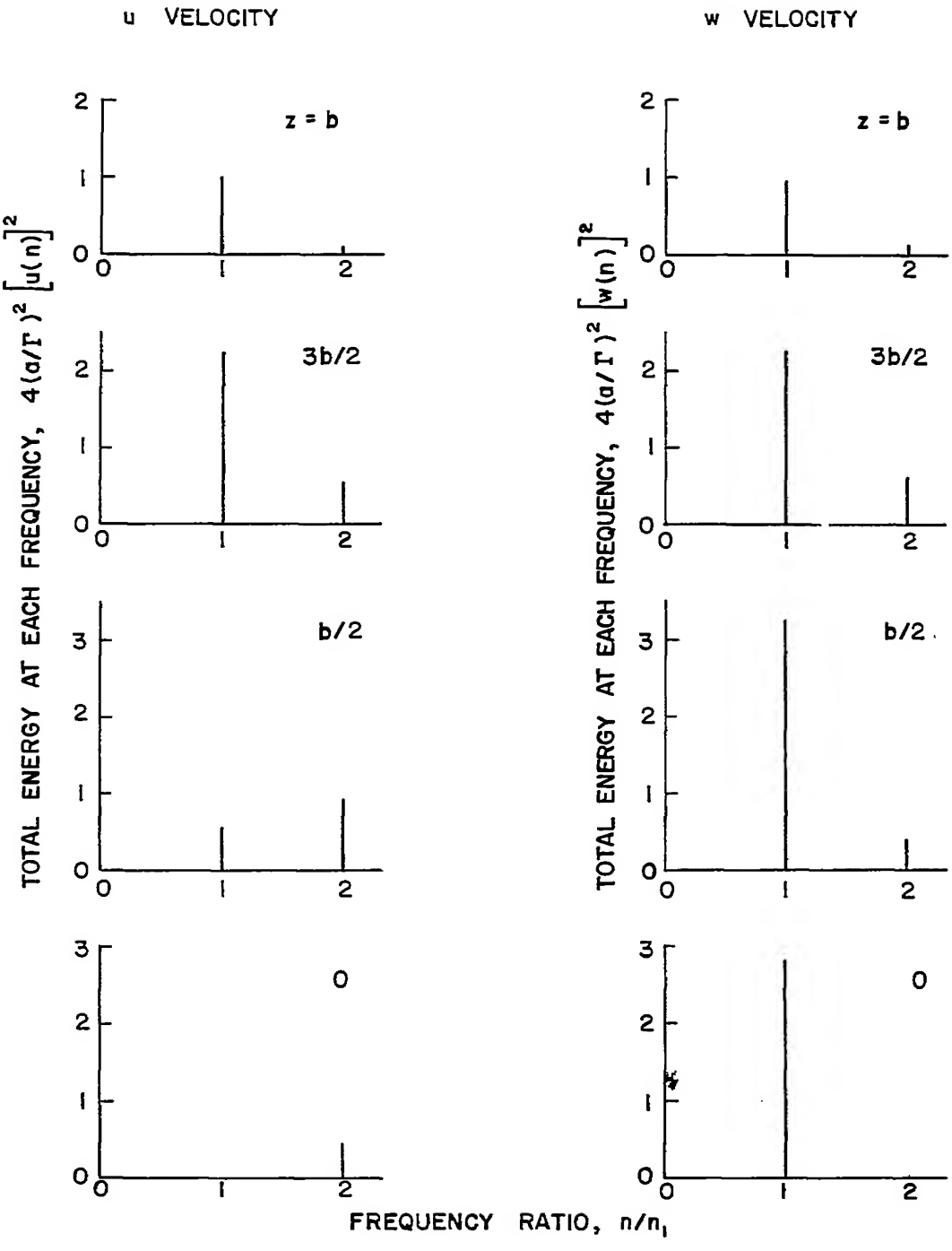

Figure 28.- Calculated frequency distribution of energy for several vertical positions in a vortex street.

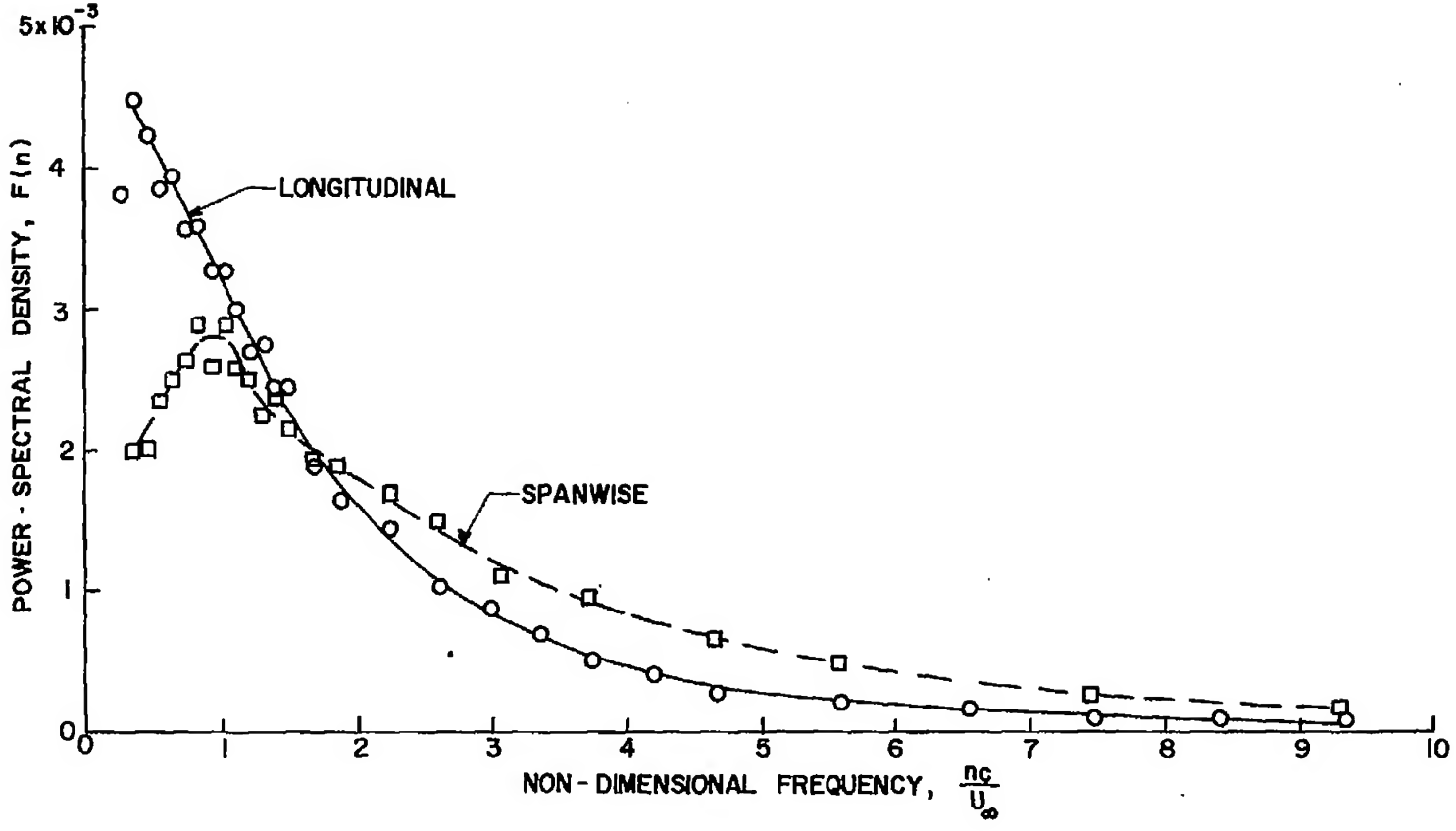

Figure 29.- Longitudinal and spanwise power spectra measured 1 chord length behind centerline of trailing edge; $\alpha = 6^{\circ}20'$, $U_{\infty} = 53.6$ fps, $z = 0$.

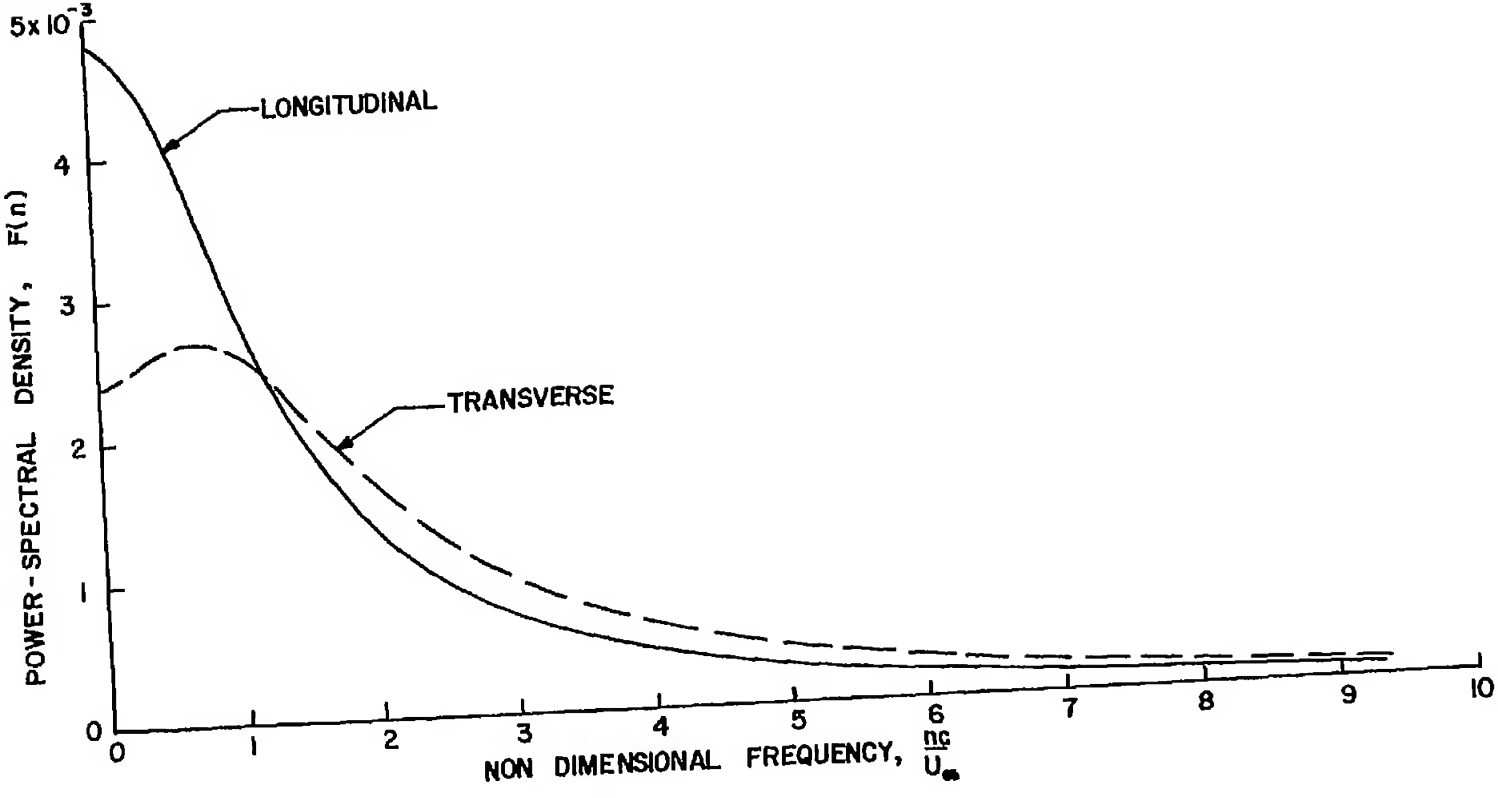

Figure 30.- Comparison of the power spectra of longitudinal and transverse velocity fluctuations in isotropic turbulence; $L/U_\infty = 1.2 \times 10^{-3}$ sec.

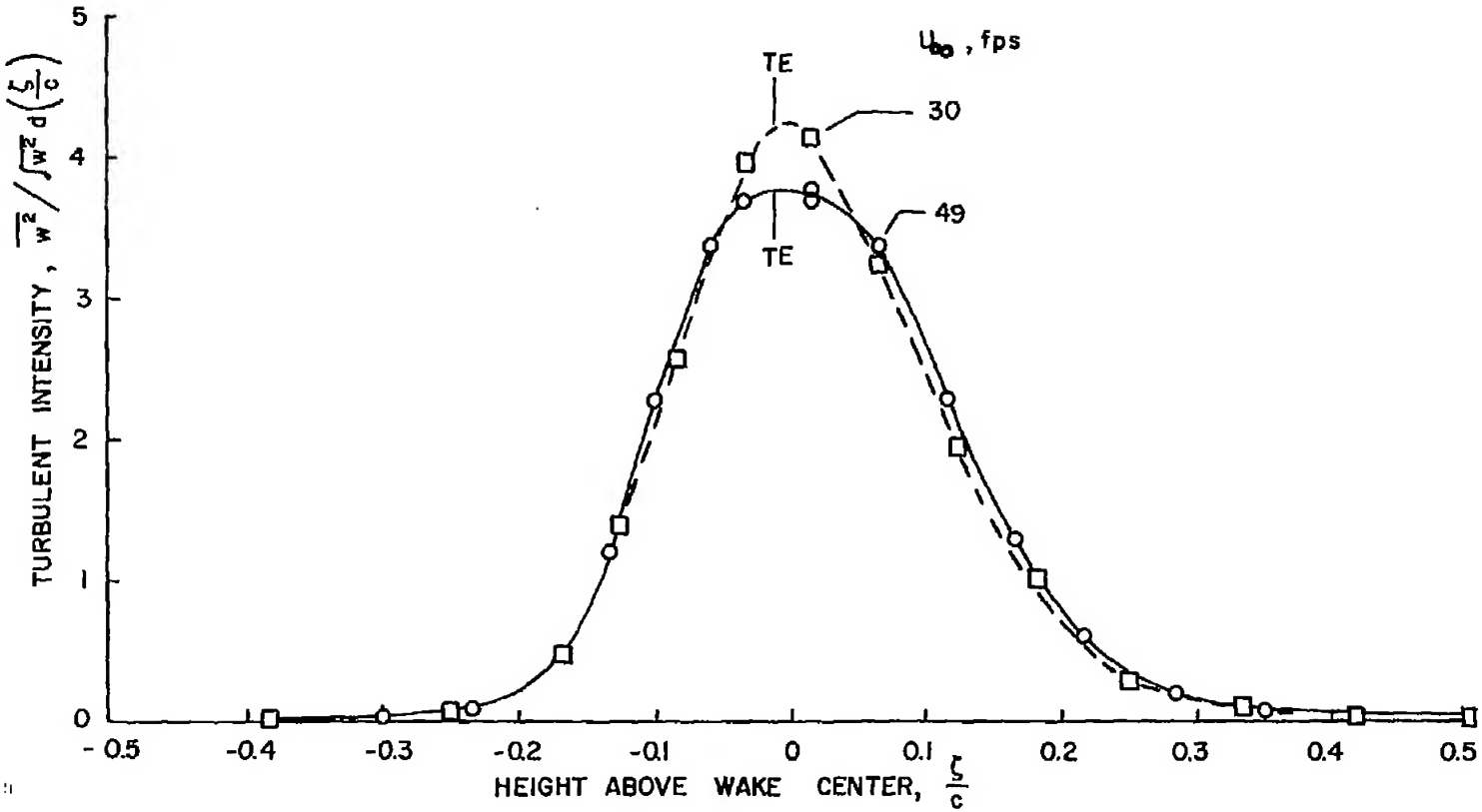

Figure 31.- Effect of free-stream velocity, U_∞, on distribution of $\overline{w^2}$ wake energy; $\alpha = 6^\circ 25'$, $x = 1c$.

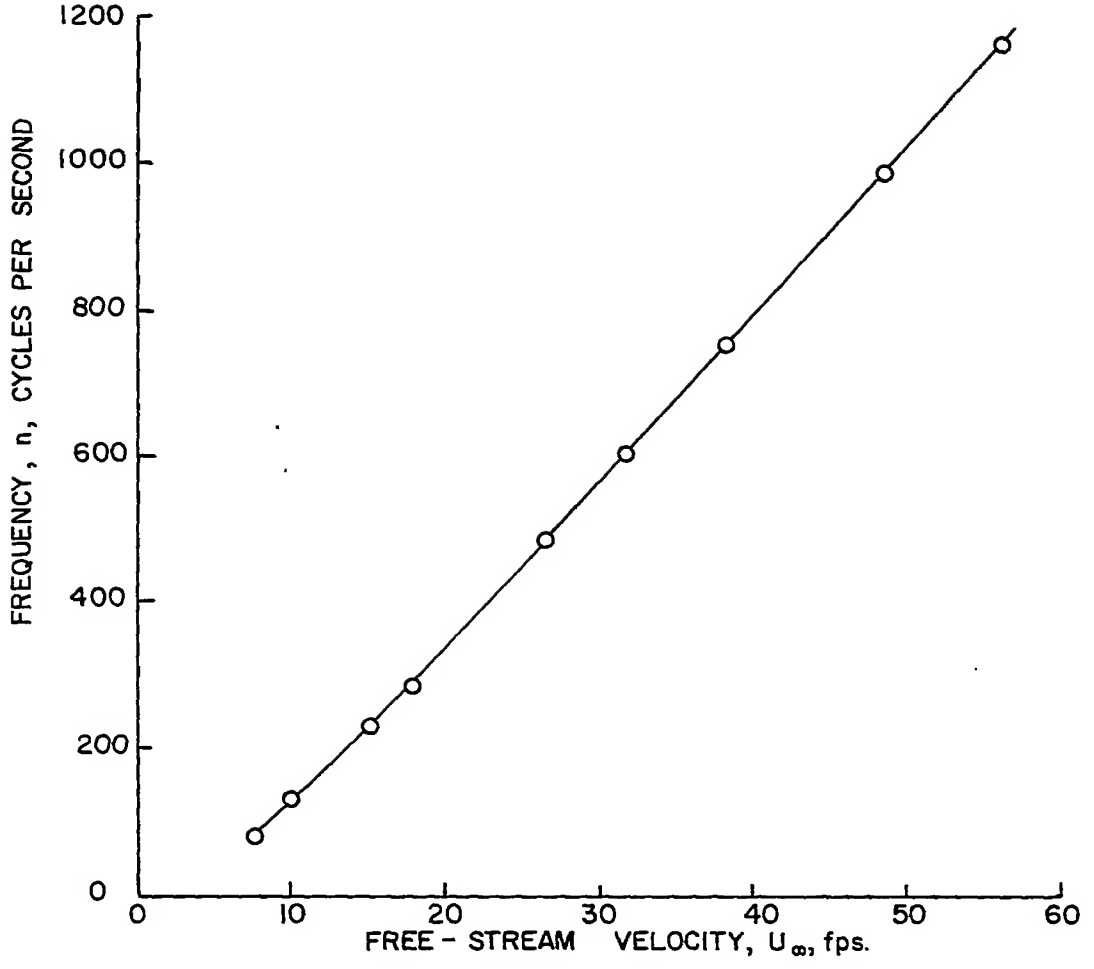

Figure 32.- Variation of frequency with free-stream velocity; $\alpha = 0$, $x = 1c$, $z = 0$.

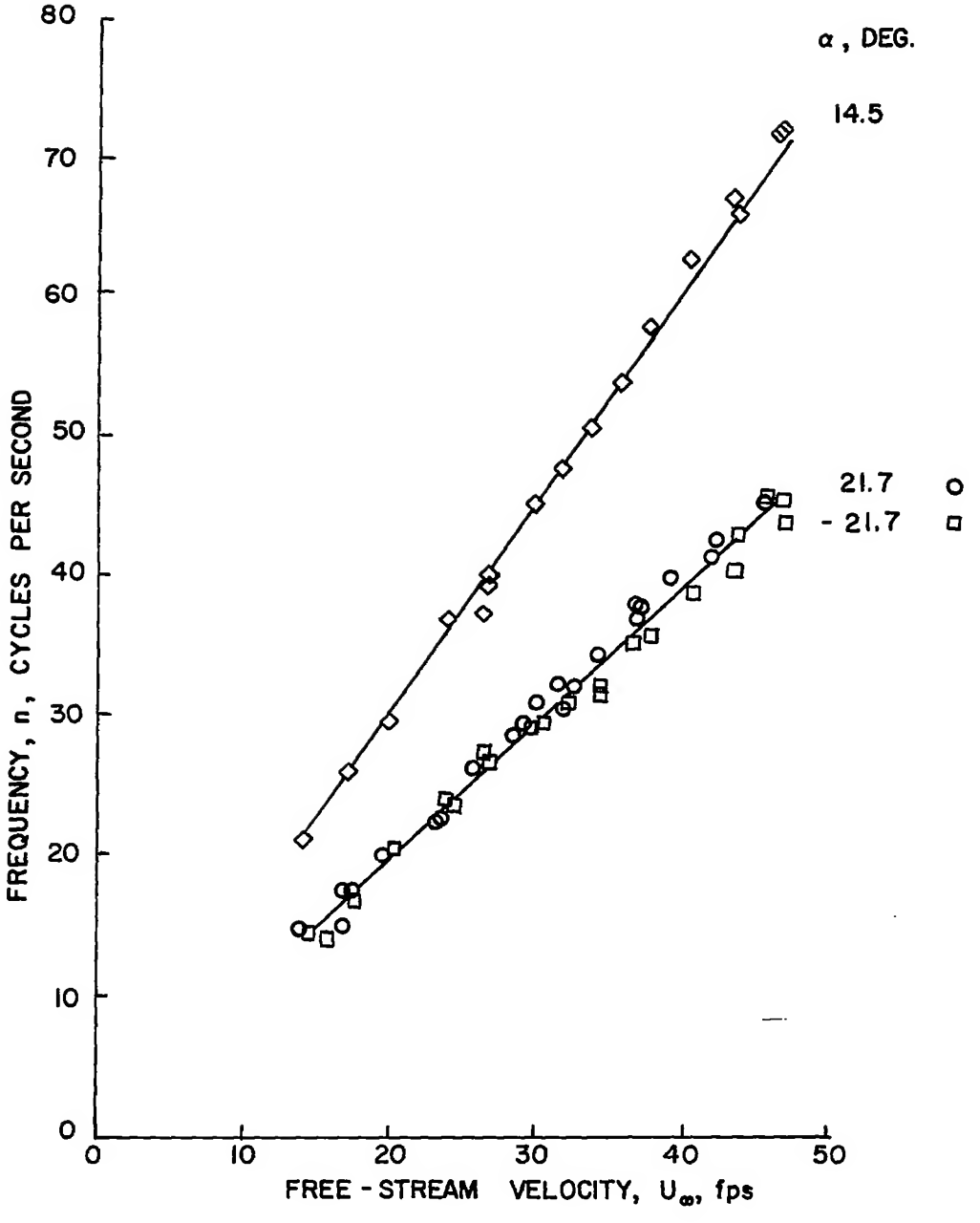

Figure 33.- Variation of frequency with free-stream velocity in the wake of stalled wing.

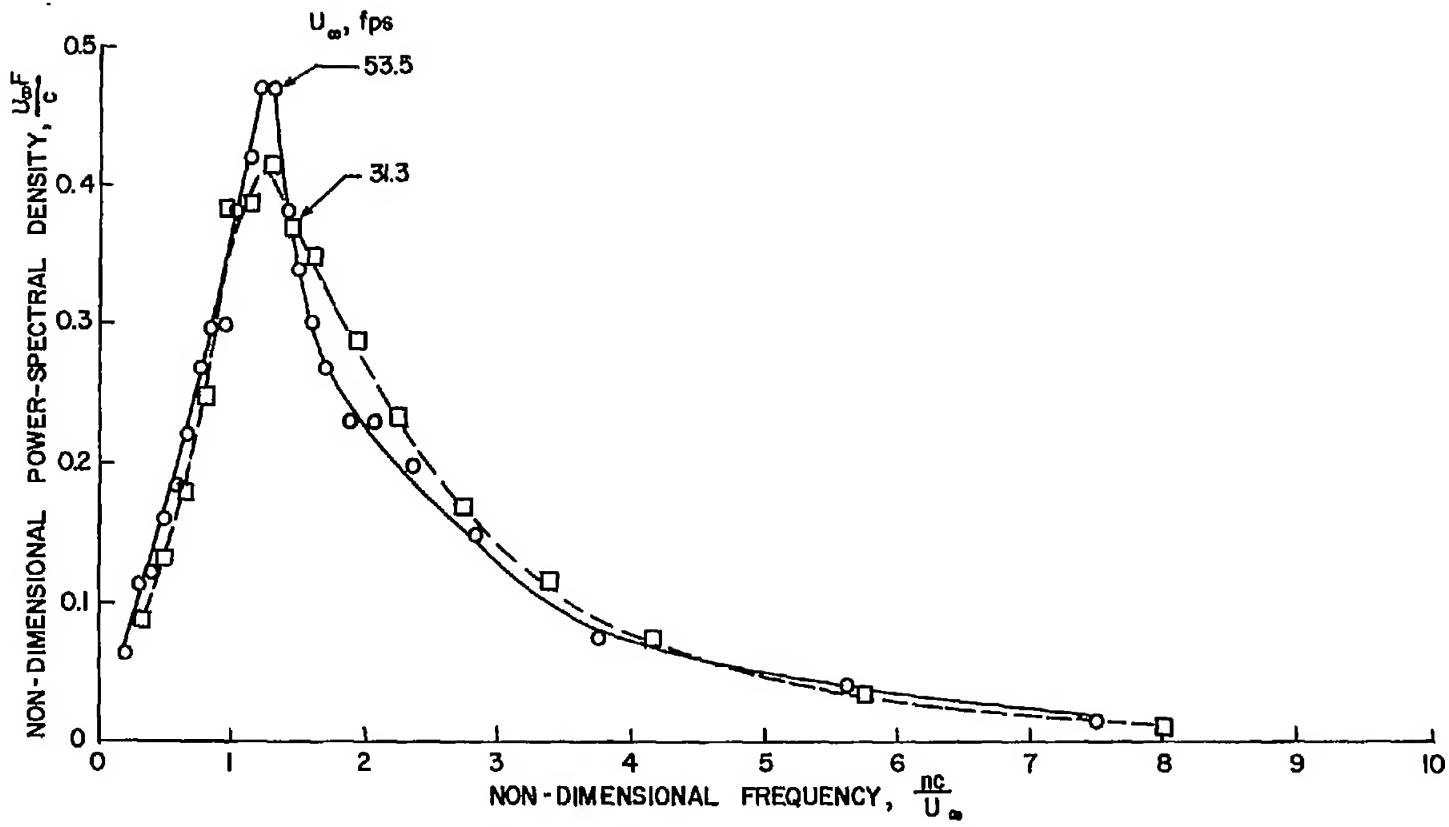

Figure 34.- Effect of free-stream velocity on the power spectrum of w^2 fluctuations; $\alpha = 6^\circ 20'$, $x = 1c$, $z = 0$.

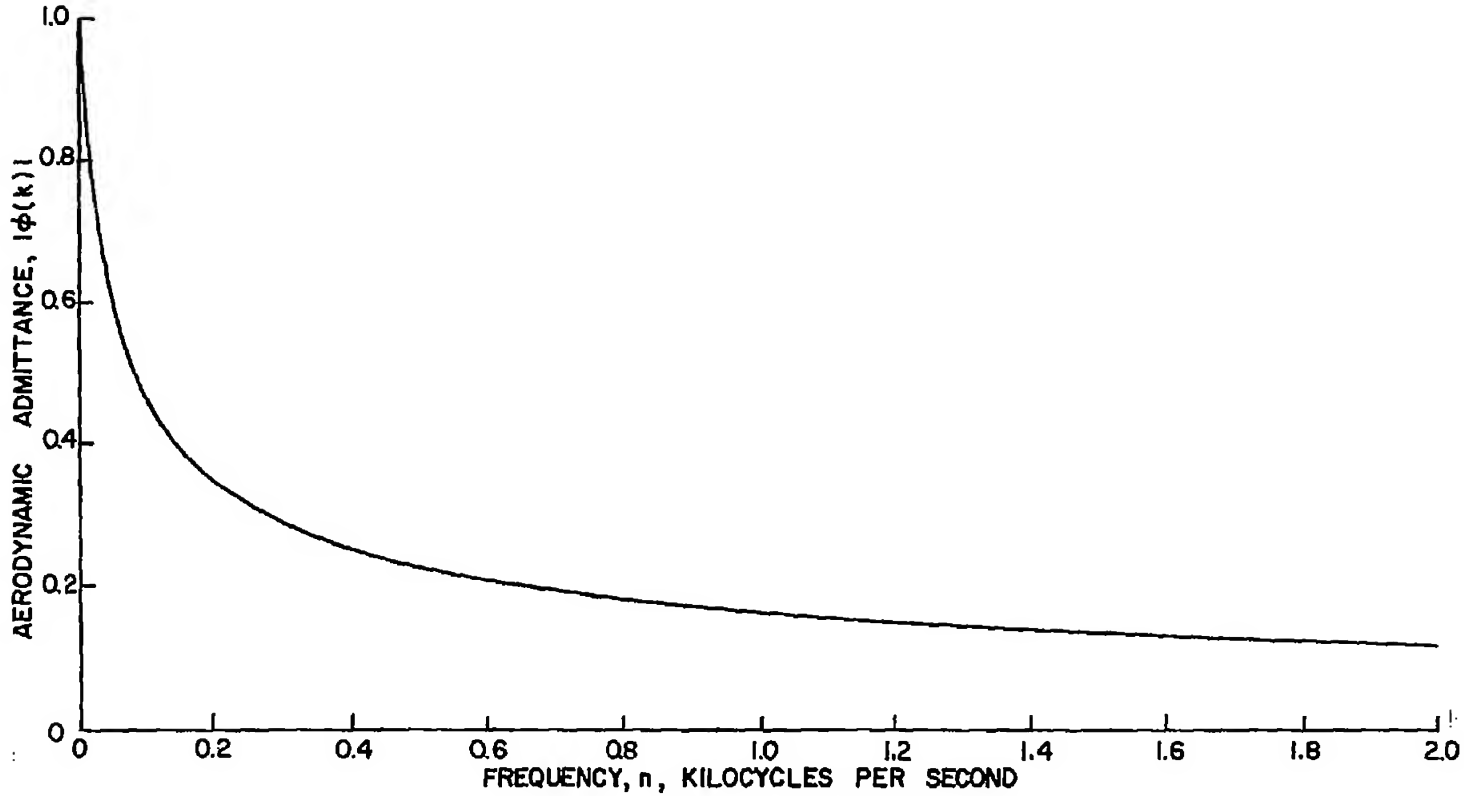

Figure 35.- Approximate aerodynamic admittance of an airfoil of 1.2 inch chord; U_∞ = 53.5 fps; $|\phi(k)|^2 = 1/(1 + 2\pi k)$.

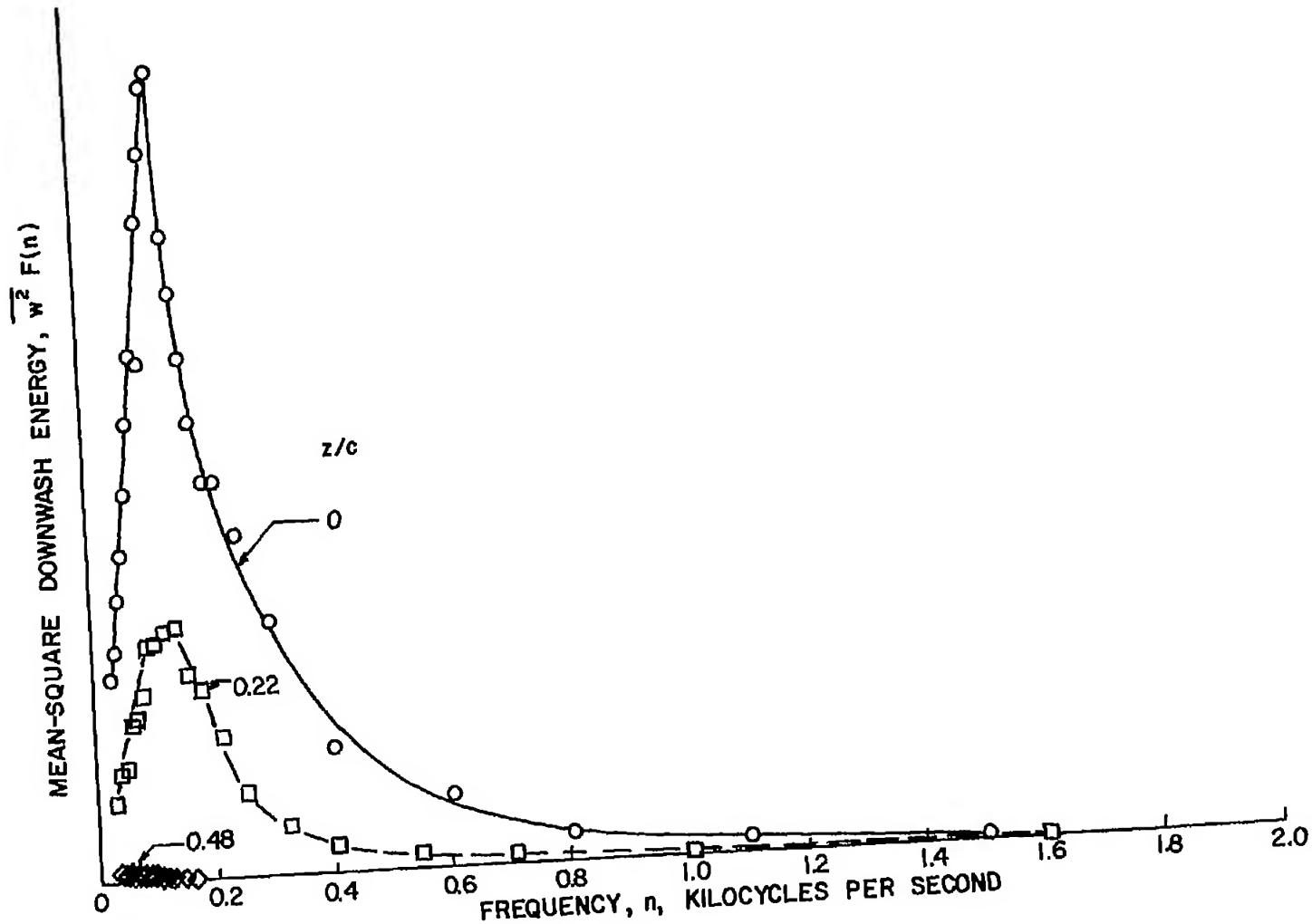

Figure 36.- Effect of tail height on the frequency distribution of mean-square downwash energy; $\alpha = 6^{\circ}20'$, $U_{\infty} = 53.5$ fps, x = 1c, half band 30 cps.

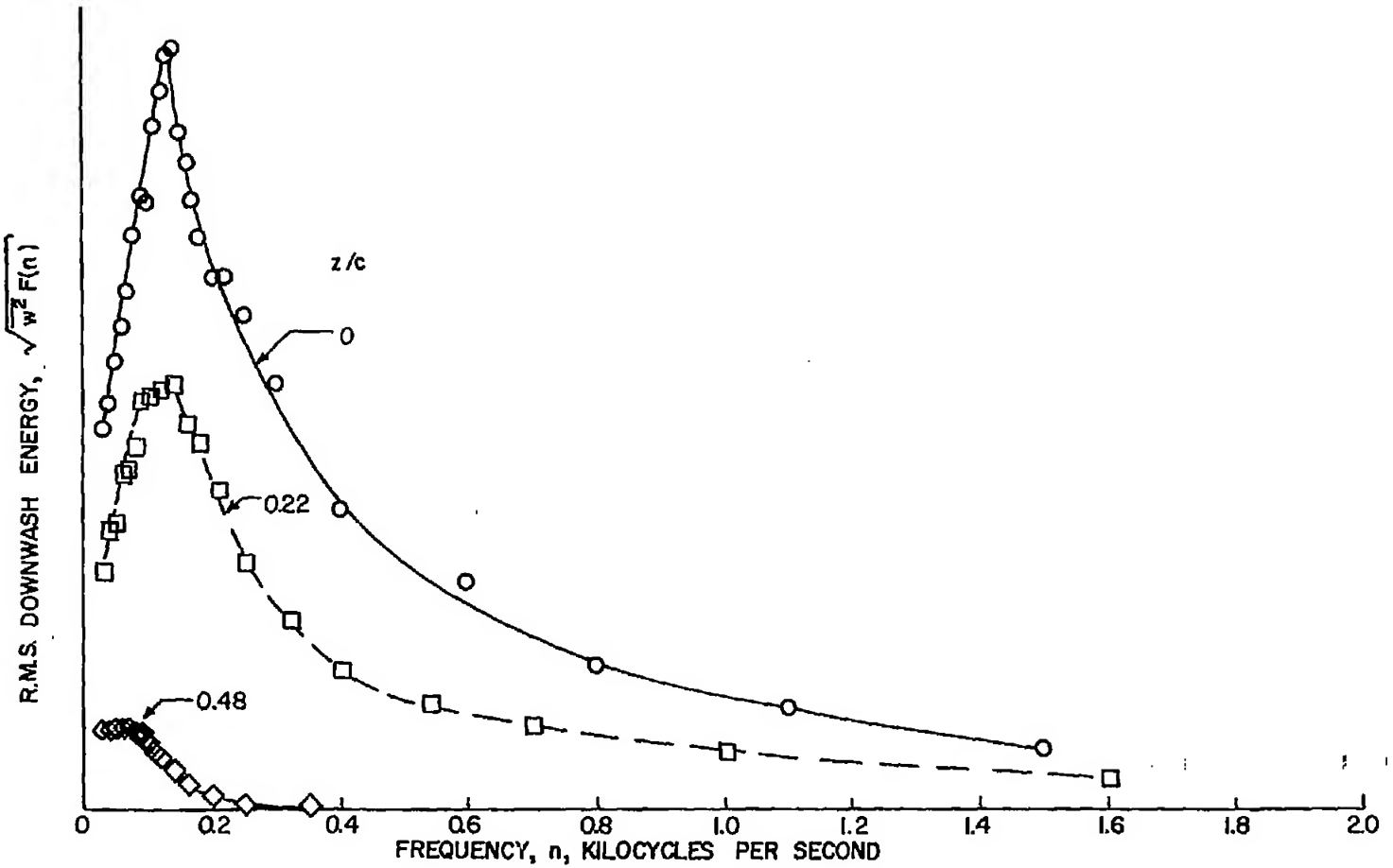

Figure 37.- Effect of tail height on the frequency distribution of RMS downwash energy; $\alpha = 6^{\circ}20'$, $U_{\infty} = 53.5$ fps, $x = 1c$, half band 30 cps.

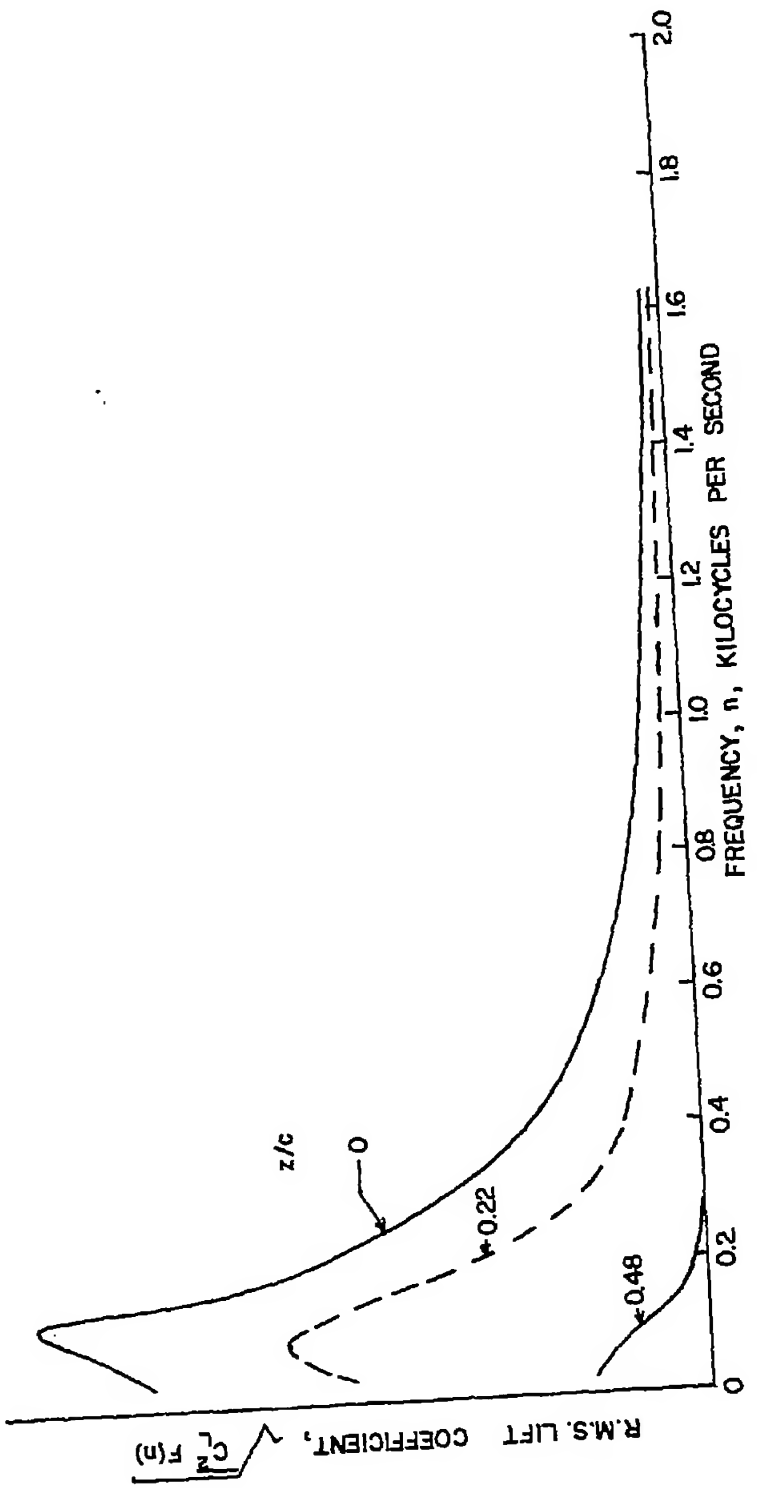

Figure 38.- Effect of tail height on the estimated frequency distribution of RMS lift on a 1.2 inch chord airfoil in the wake of a 6 inch chord airfoil; $\alpha = 6°20'$, $U_\infty = 53.5$ fps, x = 1c, half band 30 cps.